ELSEVIER

Journal of Structural Geology 26 (2004) 1317–1339

JOURNAL OF STRUCTURAL GEOLOGY

www.elsevier.com/locate/jsg

Determining the size and shape of blocks from linear sampling for geotechnical rock mass classification and assessment

J.V. Smith*

Natural Resources Engineering Discipline, RMIT University, GPO Box 2476V Melbourne 3001, Victoria, Australia

Received 3 November 2002; received in revised form 11 August 2003; accepted 24 August 2003

Abstract

Classifying and assessing geotechnical aspects of rock masses involves combining parameters in various ways, guided by empirical considerations, to derive quantitative geotechnical parameters. Geological structures and the deformation history of rocks underpin the nature of rock masses. The kinematics of a deforming rock mass may occur as sliding along throughgoing discontinuities or as distributed sliding on block faces. Distributed sliding will tend to disrupt the continuity of planar structures such that data on the size and shape of blocks is needed, rather than relying on discontinuity orientation data alone. Orientation and spacing data can be combined to provide a geometric analysis of block systems from linear samples, such as drill core. Dihedral angles and spacing of sequential pairs of discontinuities provides a sample of the size and shape of blocks that can be interpreted stereologically. Further detail can be derived by combining neighbouring intersections that enclose or partially enclose individual blocks. The shape and size of a block can be represented on a stereograph with the enclosing faces shown as poles and their perpendicular distance from an arbitrary point inside the block shown as a number. Identifying the size and shape of specific blocks rather than relying on statistical methods is beneficial to critical aspects of design such as analysing keyblocks that would be exposed during excavations. The detailed characterization of block size and shape is also a step toward interpreting the kinematics of rock mass deformation and the analysis of rock masses as ultra-close packed dilatant granular systems.

Keywords: Discontinuities; Joints; Geomechanics; Rock mass

1. Introduction

The behaviour of rock, both in engineering activities and natural processes, is influenced by the presence and characteristics of geological structures. A number of systems for quantitative geotechnical characterization of rock mass have been developed mainly through empirical engineering investigations. Structural geology, as a discipline, has much to contribute to on-going efforts to classify and assess geotechnical aspects of rock mass behaviour. In addition, structural geologists can benefit from comparing natural structures with engineering case studies that are effectively field-scale experiments where rock masses are subjected to known stresses.

Understanding of the rheology of rock masses, in general, is less advanced compared with understanding of the strength of *intact* rock. The latter is underpinned by the relevant findings of experimental rock mechanics. Similarly, the former can potentially be advanced by reference to knowledge of rock mass behaviour derived from engineering rock mechanics investigations. For example, understanding of the formation of mineralised vein and breccia systems may be enhanced by comparison with analogous deformation of rock masses in engineering works.

Reactivation of pre-existing weaknesses and discontinuities, including bedding, foliation, faults, joints and other fractures, plays a crucial role in moderating the rheology of rock in the Earth's crust (e.g. Ranalli, 2000). It is generally recognized that it is inadequate to consider geological processes in terms of rock types alone without appreciation of their rock mass characteristics. Rock masses have been classified for engineering purposes but it is necessary to seek the geological underpinnings of these empirical and practical approaches. The nature of rock types (igneous, sedimentary, metamorphic and numerous significant sub-classes) strongly influences the development and characteristics of discontinuities including inherent features (e.g. cooling cracks, bedding, foliation). Such genetic classifications do not, however, uniquely correspond to rock mass types. In particular, imposed fractures and other features of tectonic deformation contribute strongly to rock mass characteristics (e.g. Paterson, 1978; La Pointe and Hudson, 1985; Priest, 1993).

* Tel.: +61-3-9925-2184; fax: +61-3-9639-0138.
E-mail address: johnv.smith@rmit.edu.au (J.V. Smith).

0191-8141/$ - see front matter © 2004 Elsevier Ltd. All rights reserved.
doi:10.1016/j.jsg.2003.11.019

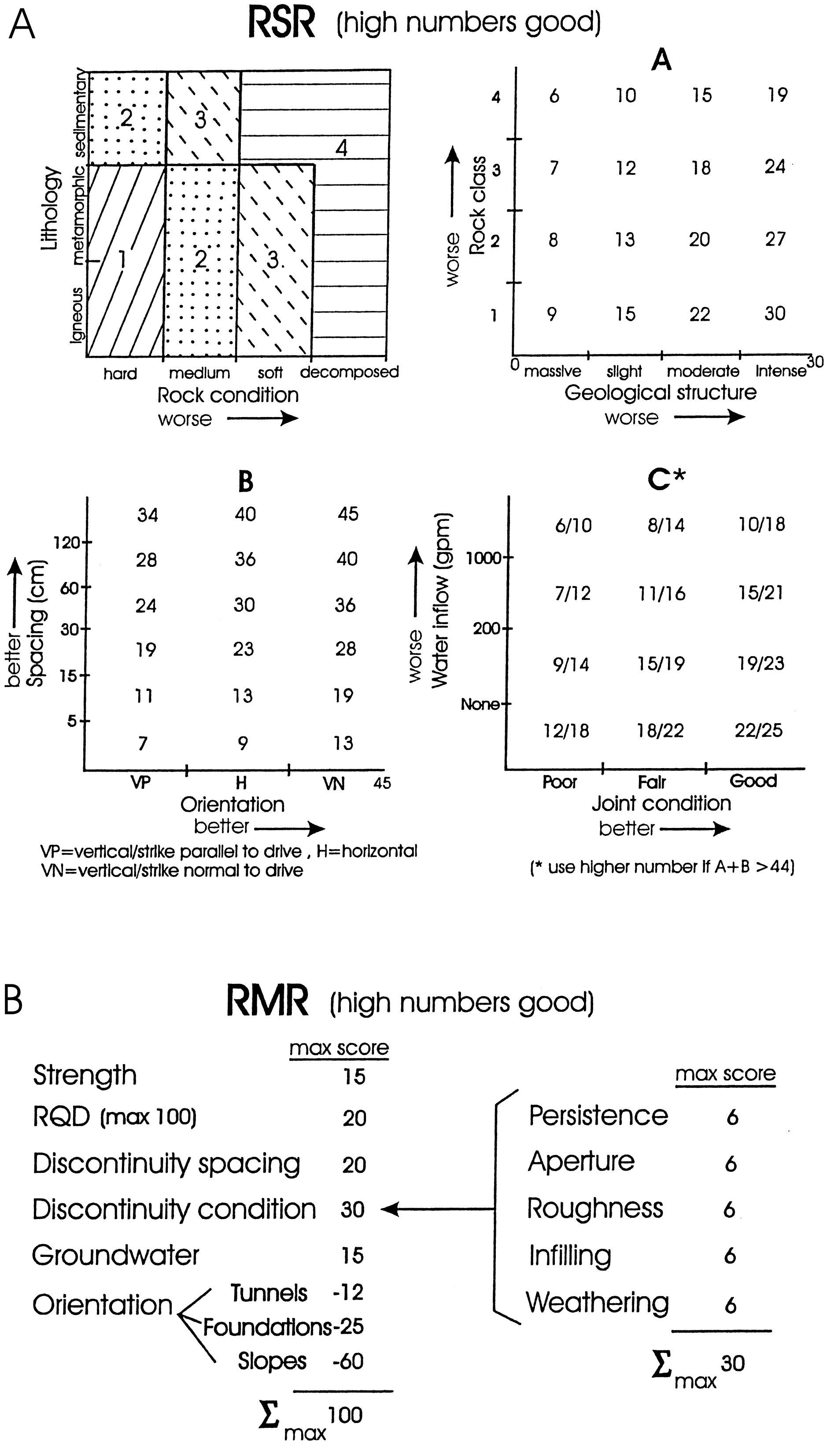

Fig. 1. Summary diagrams of selected rock mass assessment methods. (A) Rock structure rating (RSR), (B) rock mass rating (RMR), (C) Q value, (D) geological strength index (GSI). See text for sources.

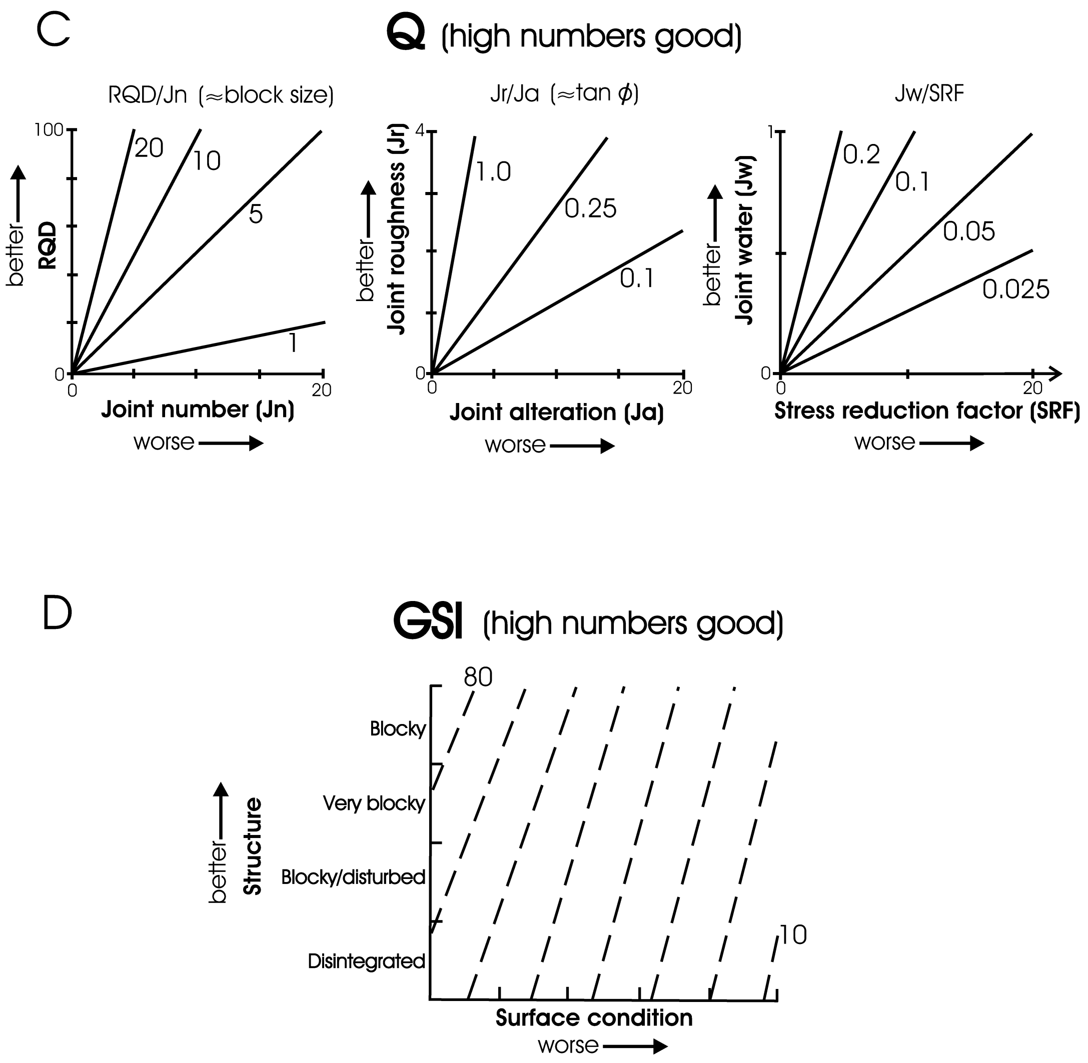

Fig. 1 (*continued*)

Current directions in research related to natural deformation of rock masses include evaluating basic criteria for interpreting the relative timing of brittle structures (e.g. Vermilye and Scholz, 1998; Peacock, 2001) and interpreting the stress history (Fry, 2001). Differences between movement of newly formed and reactivated fractures have been investigated by assessing scaling parameters that can be used to distinguish the processes (Engelder et al., 2001; Wilkins et al., 2001). Relationships between discontinuity patterns and natural stress fields have been addressed from measurements of finite strain (Gapais et al., 2000) and investigation of rock mass characteristics in active tectonic settings (e.g. Tsutsumi et al., 2001). Methods for collection of field data (e.g. Mauldon et al., 2001) and mapping techniques (e.g. 'digital mapping' of Maerten et al. (2001)) continue to be refined. Insight into the interaction of fracturing and mineral stability at elevated pressures, temperatures and hydrous conditions is being obtained from experimentation (Streit and Cox, 2000), theoretical modelling (Renard et al., 2000) and analogue materials (Streit and Cox, 2002).

Current rock mechanics research includes studies of the development of fracture systems (Schultz, 2001) and the strength and rheological behaviour of rock masses (Wu and Wang, 2001). Acoustic emission measurements are being used to study the failure process in experimental deformation (e.g. Jouniaux et al., 2001). As in structural geology, methods of data collection continue to be refined to be compatible with rigorous data analysis (Zhang and Einstein, 2000). Analytical work has noted weaknesses in practical approaches to rock mass assessment such as the use of redundant discontinuity spacing parameters (Kulatilake et al., 2001). The shearing characteristics of discontinuity surfaces remains an important aspect of investigation (Gentier et al., 2000) especially their morphology (Hopkins, 2000). Analytical models of rock mass behaviour have incorporated temperature (Guvanasen and Chan, 2000) and fluid pressure (Sitharam et al., 2001) to develop a generalized constitutive relationship. Rheological models applied to rock masses include elasto-plastic (Carranza-Torres and Fairhurst, 1999) and plastic (Pariseau, 1999). Study of the geomechanics of excavated faces does not only address processes adjacent to openings but also must consider deformation that occurs well away from excavations in ways more analogous to confined natural deformations (Shen and Barton, 1997).

Geometric interactions between discontinuity systems and excavations have been modelled numerically (Mauldon, 1995) and with probabilistic methods (Kuszmaul, 1999; Starzec and Andersson, 2002). Algorithms have been developed to generate three-dimensional patterns of polyhedral blocks necessary for numerical modelling (Jing, 2000; Lu, 2002).

In this paper the key parameters for rock mass assessment are reviewed. In particular, the relationship between discontinuity patterns and the shape and size of blocks is considered. A method of construction of individual block shapes and sizes from a neighbourhood of intersections along a sample line (e.g. drill hole) is developed. Block shapes and sizes can be illustrated on a stereograph as poles to block faces together with perpendicular distances to a single reference point within the block.

2. Geotechnical rock mass assessment systems

Selected rock mass assessment systems commonly used in geotechnical practice will be briefly reviewed with emphasis on the approach each takes to the selection and combination of parameters.

2.1. Rock structure rating (RSR)

In this system numerical scores are derived from parameter groups A, B and C (Fig. 1A). Parameter A is based on lithology and the main factor amending these values is the presence of folding or faulting, which can decrease the score by as much as two-thirds. Parameter B is based on scores in a matrix based on discontinuity spacing versus orientation of discontinuities with respect to excavations (tunnels). Parameter C includes the condition of joint (discontinuity) surfaces from tight and cemented to weathered and altered (Wickham et al., 1974, cited in Afrouz, 1992).

2.2. Rock mass rating (RMR)

In this system tabulated scores (total: 0–100) for selected properties are summed (Fig. 1B). Final scores are adjusted depending on the type and orientation of an excavation relative to structures present. The scores have been progressively modified as case study data from a range of applications have increased. Of the six parameters used, both the rock quality designation (RQD) and joint spacing relate to the pattern of discontinuities. The surface condition of a joint (discontinuity) is scored from 0 to 30, the lowest class being greater than 5 mm of infilling of gouge (Bieniawski, 1989).

2.3. Rock mass quality (Q)

This system was devised for tunnelling support design and uses the product of the ratios of selected parameters (Fig. 1C). A discontinuity spacing parameter (RQD) is divided by the joint set number to give an estimate of block size. A joint roughness parameter is divided by a joint alteration parameter to give an index inferred to be correlated with inter-block shear strength. Discontinuity surface conditions are determined and systematized as the joint alteration number (J_a). In this system there are three main classes where (1) the walls are in contact, (2) the walls would achieve contact before 10 cm of movement, and (3) walls would not come into contact during shearing. Subclasses are determined based on the nature of the infill material. In its application, this method incorporates an aspect of time dependent rheology in the 'stand up time' design parameter. The system incorporates factors that relate the observed structural orientations to the shapes and orientations of proposed excavations (Barton et al., 1974; Barton, 1999).

2.4. Hoek–Brown rock mass strength criterion

This approach uses confined and unconfined (UCS) compressive strength of intact rock together with a geological strength index (GSI) to characterize the strength of rock masses (Fig. 1D). This method is only applicable to situations where the excavation is large relative to discontinuity spacing as it does not address the orientations of discontinuities but assumes isotropic rock mass characteristics. The GSI is a number derived from a matrix with parameters of structure and discontinuity surface condition. Within the structure parameter, the method recognises that rocks that have undergone deformation tend to have more problematic discontinuity patterns. Surface conditions including slickensides and clay coatings and fillings are recognised as the most problematic (e.g. Hoek and Brown, 1997).

2.5. Correlation between systems

There have been numerous efforts made to establish correlation factors between rock mass assessment systems (e g. Afrouz, 1992). There have also been studies assessing the influence of different types of sampling, such as core versus in situ measurements (Cameron-Clarke and Budavari, 1981) or different interpretations by practitioners (Fookes, 1997). Although the emphasis in these geotechnical rock assessment methods is on practical techniques with empirical validation, scientific considerations of the physical meaning of derived parameters and an

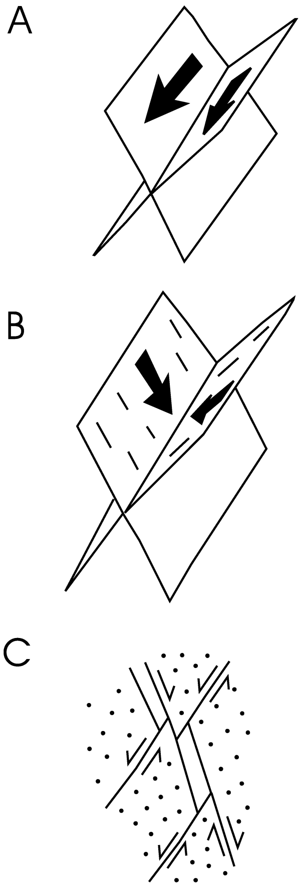

Fig. 2. (A) Multisurface unidirectional slip in a rock mass. (B) Multisurface multidirectional slip in a rock mass. (C) Multisurface multidirectional slip of blocks (stippled) leads to dilation of a rock mass (unstippled) and offsetting of discontinuities.

understanding of the origin of rock mass structures can potentially make a contribution to rock mass assessment and classification.

2.6. Deformation modulus

Although not a comprehensive geotechnical rock mass assessment, the stress–strain relationship of a rock mass, commonly referred to as the deformation modulus, is a single parameter that is potentially as important as it is difficult to determine. He (1993) reviewed 258 measured deformation moduli determined from experiments and relaxation during tunnelling. Numerical models are being developed but there are many different ways of incorporating the rock mass behaviour. According to Cunha (1993) "The fundamental unit of analysis should be then the systematic joint sets, whose properties are basic input parameters for model analysis". These joints can be modelled in different ways, for example, Moon and Kim (1993) regard joints as soft layers embedded in intact rock. The ratio of rock mass to intact rock modulus or modulus contrast number, Poison's ratio and modulus anisotropy are important related considerations.

Two approaches to the analysis of the deformability of rock masses are (1) equivalent continuum models, and (2) explicit methods (Priest, 1993, p. 322). Equivalent continuum models do not account for orientation of discontinuities and the resulting non-uniform stresses. Models that state the applied stress orientations are not strictly models of the rock mass but of the interaction of the rock mass and a particular stress (Priest, 1993, p. 330).

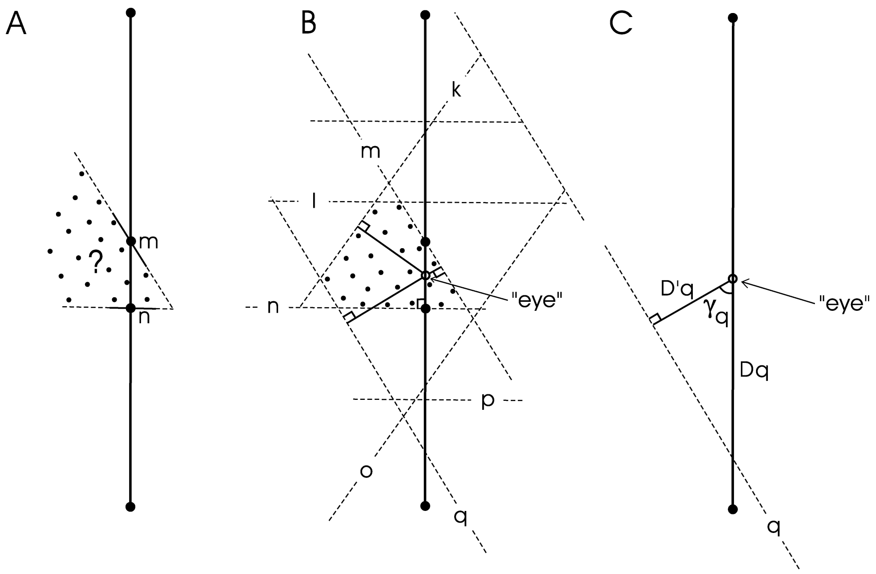

Fig. 3. (A) The direct intersections of a block (designated m and n) provide limited data on the size and shape of a block. (B) In a system of persistent discontinuities most block faces will intersect the sample line. (C) The mid-point between m and n ('eye' of the block) is chosen as an arbitrary reference point from which distances to block faces can be computed.

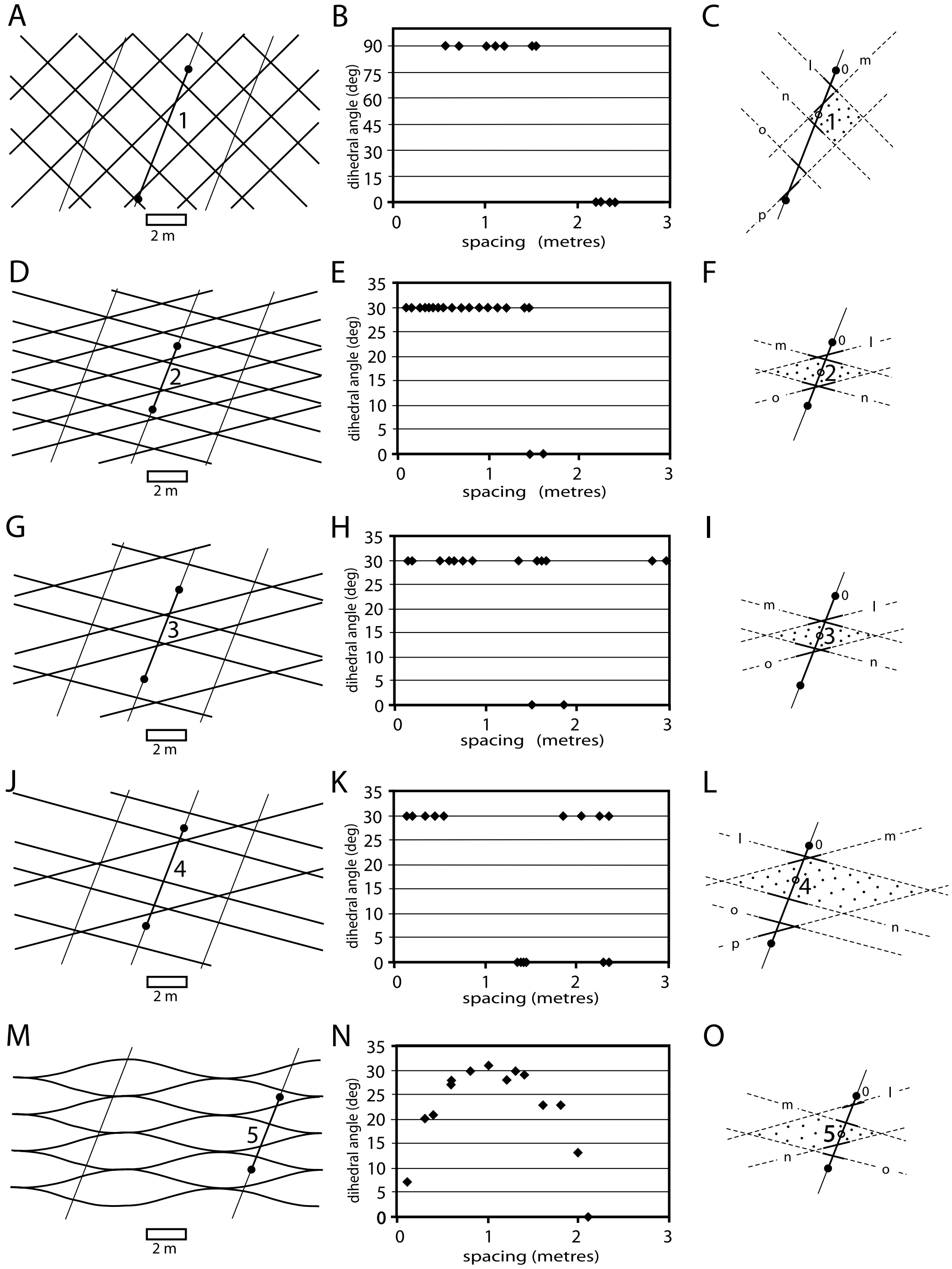

Fig. 4. Two-dimensional models of discontinuity patterns. (A) A regular pattern of orthogonal discontinuities with arbitrary sample lines (fine lines) and a block defined by the discontinuity pattern (1). (B) The pattern of dihedral angle versus spacing for an arbitrary linear sampling of a regular orthogonal discontinuity system. The maximum spacing occurs for parallel structures. (C) Block 1 can be constructed from oriented intersections in a linear sample (e.g. drill core). Intersections where the sample line enters and exits the block are designated m and n, respectively. Intersections are designated in alphabetical order above and below the block. (D) A regular pattern of oblique discontinuities with arbitrary sample lines (fine lines) and a block defined by the discontinuity pattern (2). (E) The pattern of dihedral angle versus spacing for an arbitrary linear sampling of a regular oblique discontinuity system is illustrated. (F) Construction of block 2 from intersections on the sample line. (G) and (J) Irregular discontinuity patterns. (H) and (K) Irregularly spaced and unequally represented systems where the spacing and representation of parallel structures varies. (I) and (L) Constructions of blocks 3 and 4 from sample intersections. (M) Regular anastomosing discontinuities. (N) An arbitrary linear sampling of a regular anastomose discontinuity system is distinctive in that the maximum dihedral angle occurs at an intermediate spacing. (O) Constructed block 5 only approximates its true size and shape.

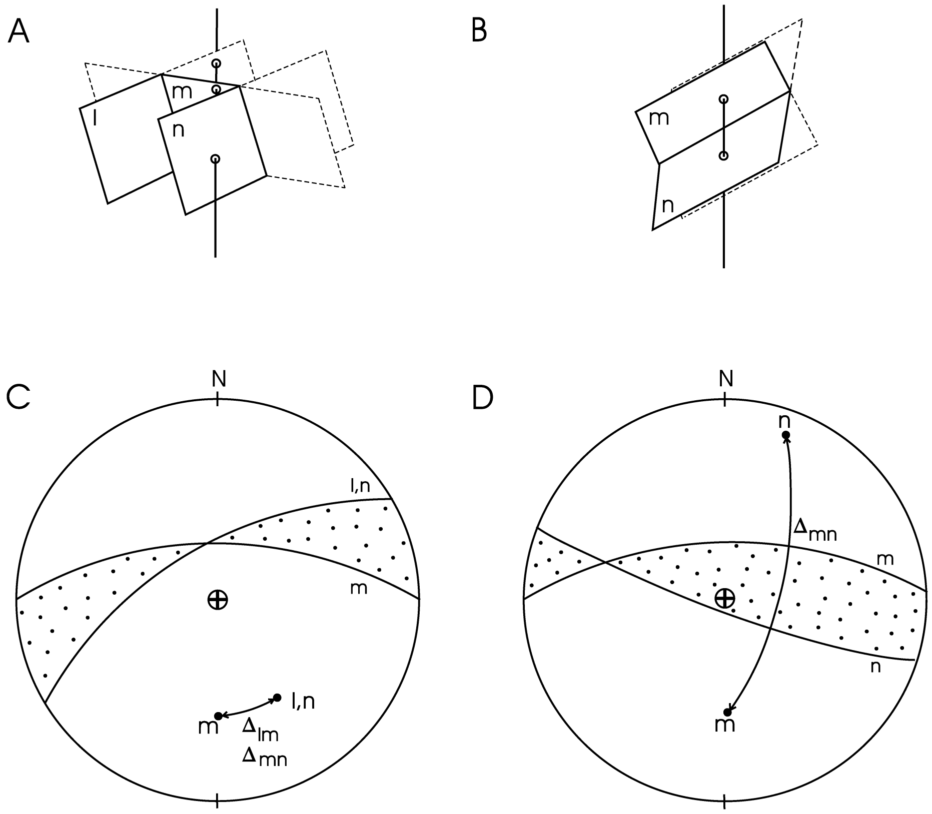

Fig. 5. (A) In three-dimensions the dihedral angle (Δ) between planes may have an acute (A) and obtuse (B) expression. These possibilities can be differentiated on a stereograph by the location of the sample line (circle) relative to the acute (stippled) and obtuse (unstippled) fields between the planes (m and n). (C) For intersections on either side of the eye of the block (e.g. m and n) the block corner is acute if the sample line is in the obtuse field. For planes on the same side of the eye of the block (e.g. l and m) the block corner is obtuse if the sample line is in the obtuse field.

3. Geotechnical analysis of discontinuities

Structural geological investigations are characterized by emphasis on determining the geometry or pattern of geological features, determining the movements involved in their formation (kinematics) and interpreting the forces involved in their formation (dynamics) (e.g. Ramsay, 1967). Together these findings are used to develop models of the origin of geological structures. Historic and on-going research into the occurrence and origin of geological structures provides a firm scientific framework for understanding rock masses. Although brittle structures have not been ignored, the emphasis has traditionally been on the ductile structures, which reflect the more deep-seated crustal deformations. For structural geological findings to be fully applied in engineering work it is necessary for structural geologists to be aware of the ways in which engineers prefer to process and interpret rock mass data.

Based on the four rock mass assessment techniques outlined above, structural parameters can be grouped together under the main headings of orientation/pattern of discontinuities, morphology of discontinuity surfaces and geological conditions of rock masses. These parameters include the orientation of individual planar structures, the spacing of parallel sets of structures and the recognition of multiple sets of structures to form a three-dimensional network. The network of structures also defines the size and shape of blocks within the rock mass. Orientation data for engineering purposes is typically collected and displayed on stereographs. In the RSR and RMR systems, orientations are incorporated according to their favourability to a given excavation. In the Q system, orientation is incorporated by using physical parameters of the discontinuity set with the least favourable orientation. In contrast, the Hoek–Brown approach assumes isotropy. The use of favourability of orientation implies that particular failure mechanisms are being considered. Falls and slides are the two main mechanisms considered.

A great deal of engineering geology research has focussed on sliding along single or multiple planes. The kinematics considered is typically that of a single displacement vector shared by the sliding planes with detachment from the greater rock mass by along other discontinuity planes (Fig. 2A). Toppling failures occur primarily by detachment on discontinuities, and have also been investigated in detail. More complex deformations, involving multiple displacement vectors throughout a rock mass leading to bulk deformation have also been investigated (Fig. 2B). Multidirectional slip will produce incompatible displacements of blocks and therefore dilatancy (Fig. 2C),

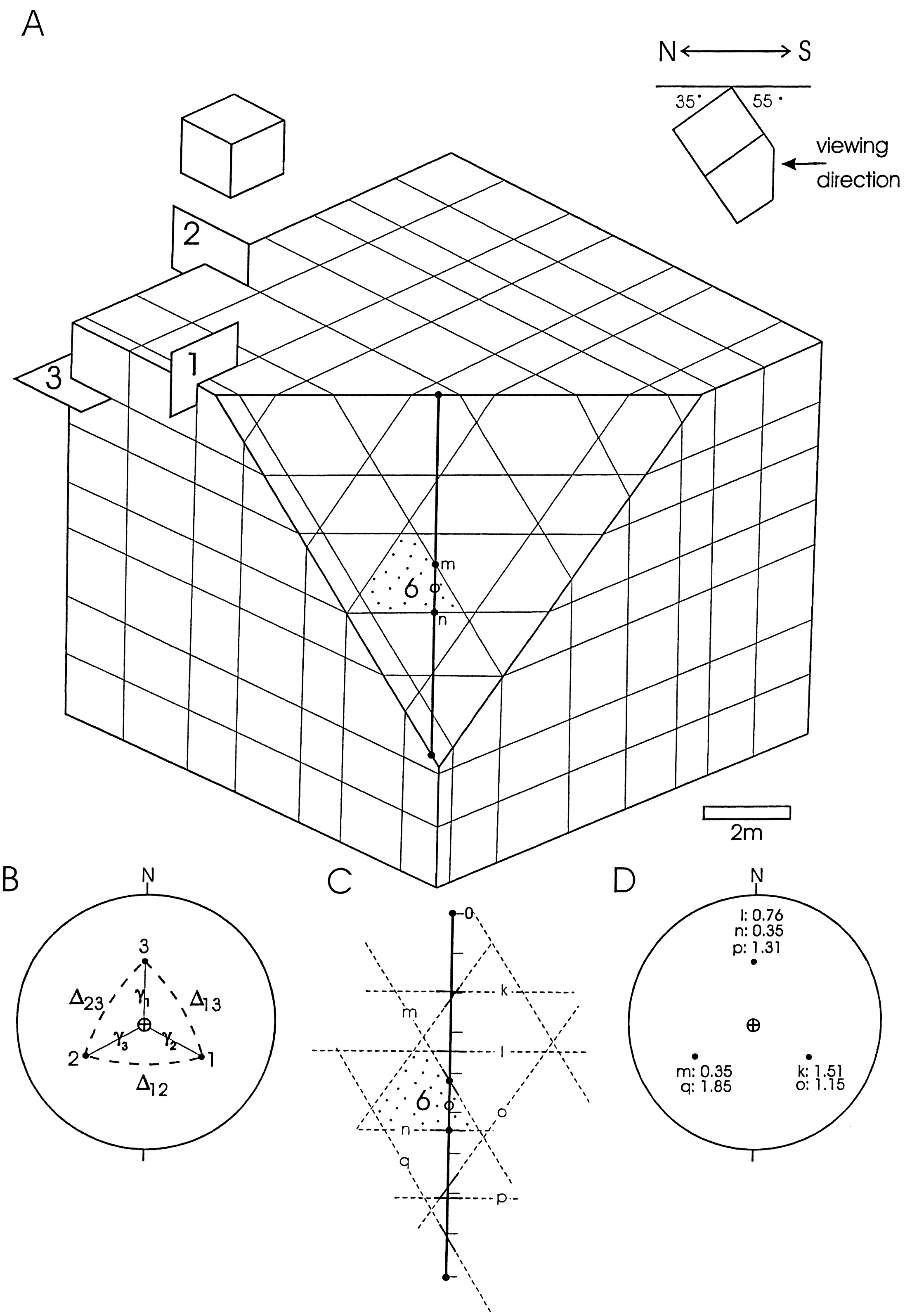

Fig. 6. (A) A schematic diagram of three mutually orthogonal discontinuity sets (numbered) cut by a vertical plane (triangular face in centre) to show intersections with the discontinuities. An arbitrary vertical sample line (bold line with terminal bulbs) enters block 6 through face m and leaves through face n. (B) A stereograph (equal angle projection is used throughout) of discontinuities in (A) showing the dihedral angles between faces (Δ) and the angle between poles to faces and the vertical sample line (γ). (C) An extract from (A) showing the construction of block 6 (stippled) from intersections of neighbouring discontinuities (dashed lines) along the sample line. Intersections are labelled in alphabetical order along the sample line such that m and n are the faces at which the sample line enters and leaves the block, respectively. These designations are 'floating' such that intersection 'k' for any block is two intersections before the sample line enters the block. (D) A stereograph showing the orientation of intersected discontinuities and their perpendicular distance (metres, see Table 1) from the 'eye' (mid point between m and n) of block 6. This diagram summarizes the shape and size of the block. Intersection p is redundant.

Table 1
Model and field data for blocks as labelled in the figures

Block	Face	Intersection position (m) (relative to zero)	Intersection position (m) (relative to 'eye')	γ (°)	D' (m)
1	l	0.75	−1.59	25	1.44
	m	1.75	−0.59	65	0.25
	'eye'	2.34	0		
	n	2.94	0.59	25	0.53
	o	5.06	2.72	25	2.47
	p	6.41	4.06	65	1.72
2	l	0.69	−0.94	37	0.75
	m	0.94	−0.69	7	0.68
	'eye'	1.63	0		
	n	2.31	0.69	7	0.68
	o	2.44	0.81	37	0.65
3	l	1.25	−0.86	37	0.69
	m	1.41	−0.7	7	0.69
	'eye'	2.11			
	n	2.81	0.7	7	0.69
	o	2.97	0.86	37	0.69
4	l	0.59	−1.22	7	1.21
	m	0.75	−1.06	37	0.85
	'eye'	1.81	0		
	n	2.88	1.06	7	1.05
	o	4.13	2.31	7	2.29
	p	4.63	2.81	37	2.24
5	l	0.5	−1.55	38	1.22
	m	1.47	−0.58	5.5	0.58
	'eye'	2.05	0		
	n	2.63	0.58	36	0.47
	o	3.22	1.17	6.5	1.16
6	k	2.1	−2.64	55	1.51
	l	3.41	−1.33	55	0.76
	m	4.13	−0.61	55	0.35
	'eye'	4.74	0		
	n	5.35	0.61	55	0.35
	o	6.75	2.01	55	1.15
	p	7.02	2.28	55	1.31
	q	7.97	3.23	55	1.85
7	l	0.77	−3.25	36	2.63
	m	3.85	−0.17	83	0.14
	'eye'	4.02	0		
	n	4.19	0.17	83	0.14
	o	8.01	3.99	36	3.23
8	k	0.52	−2.15	61	1.04
	l	1.12	−1.55	62	0.73
	m	1.5	−1.17	31	1
	'eye'	2.67	0		
	n	3.84	1.17	70	0.4
	o	4.65	1.98	30	1.71
	p	6.76	4.09	80	0.71
	q	7.83	5.16	81	0.81
9	l	0.36	−1.15	36	0.93
	m	0.83	−0.68	68	0.25
	'eye'	1.51	0		
	n	2.19	0.68	7	0.67
10a	k	0.39	−0.95	88	0.03
	l	0.86	−0.49	39	0.38
	m	1.05	−0.3	14	0.29
	'eye'	1.35	0		
	n	1.64	0.3	18	0.29
	o	1.93	0.59	12	0.58
	p	1.99	0.64	17	0.61
	q	2.32	0.97	19	0.92

Table 1 (*continued*)

Block	Face	Intersection position (m) (relative to zero)	Intersection position (m) (relative to 'eye')	γ (°)	D' (m)
10b	k	0.39	−0.57	3	0.57
	l	0.5	−0.45	32	0.38
	m	0.72	−0.23	66	0.09
	'eye'	0.95	0		
	n	1.19	0.23	39	0.18
	o	1.55	0.59	32	0.5
	p	1.92	0.97	35	0.79
11	j	0.41	−0.69	60	0.35
	k	0.41	−0.69	24	0.63
	l	0.7	−0.4	44	0.29
	m	1.03	−0.06	48	0.04
	'eye'	1.1	0		
	n	1.16	0.06	55	0.03
	o	1.4	0.3	17	0.29
12	m	1.05	−0.21	13	0.2
	'eye'	1.27	0		
	n	1.48	0.21	10	0.21
13	l	0.99	−0.68	31	0.58
	m	1.14	−0.53	46	0.37
	'eye'	1.66	0		
	n	2.19	0.53	40	0.41

which Barton (1999) identified as the major control on rock mass deformation. This process has been recognised in experimental models of rock mass deformation where local crushing zones due to stress concentrations occurred together with local dilation (Priest, 1993, p. 334). Detailed kinematics of complex rock masses is an area in which structural geology analyses of complex brittle deformations could contribute to an understanding of inferring probable bulk displacements for complex rock mass configurations.

Spacing of discontinuities is a commonly used rock engineering parameter (Franklin et al., 1971). It is incorporated as a unit of length measured perpendicular to sequential discontinuities (e.g. RSR), the rock quality designation (RQD: percentage of a linear sample with intervals exceeding 10 cm between discontinuities, e.g. Q system) or both types of measure (e.g. RMR). For linear samples spacing can be corrected for orientation bias.

The pattern of discontinuities (other than their spacing) is only explicitly assessed in the Q system with the number of joint sets being determined from a stereograph. The J_n scores in the Q system are on an arbitrary scale up to 20. For example, 2 joint sets plus random joints receives a score of 6. Although sets of planar structures are familiar in structural geology there is no equivalent to the joint number parameter. An alternative approach to focusing on discontinuities is to consider the attributes of the blocks of rock separated by the discontinuities. In the Q system block size is estimated by dividing RQD by J_n. Since neither of these values is in physical units the resulting correlation with block size is indirect.

The Hoek–Brown approach has four classes of structure based on shapes of blocks: blocky (cubic blocks defined by

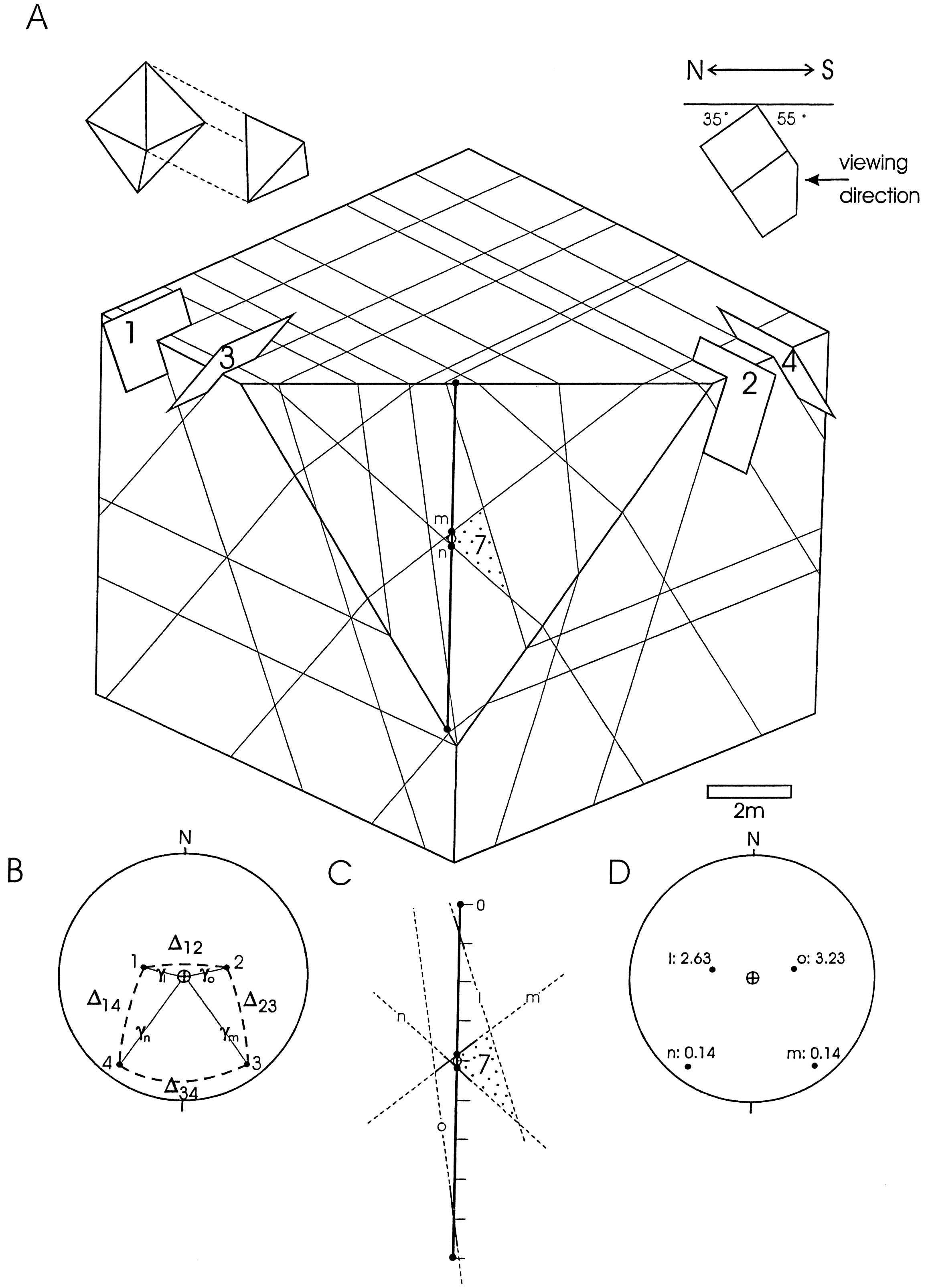

Fig. 7. (A) A schematic diagram of four octahedral/tetrahedral discontinuity sets (numbered) cut by a vertical plane (triangular face in centre) to show intersections with the discontinuities. An arbitrary vertical sample line (bold line with terminal bulbs) enters block 7 through face m and leaves through face n. (B) A stereograph (equal angle projection is used throughout) of discontinuities in (A) showing the dihedral angles between faces (Δ) and the angle between poles to faces and the vertical sample line (γ). C) An extract from (A) showing the construction of block 7 (stippled) from intersections of neighbouring discontinuities (dashed lines) along the sample line. Intersections are labelled as for Fig. 6. (D) A stereograph showing the orientation of intersected discontinuities and their perpendicular distance (metres, see Table 1) from the 'eye' (mid point between m and n) of block 7. This diagram summarizes the shape and size of the block.

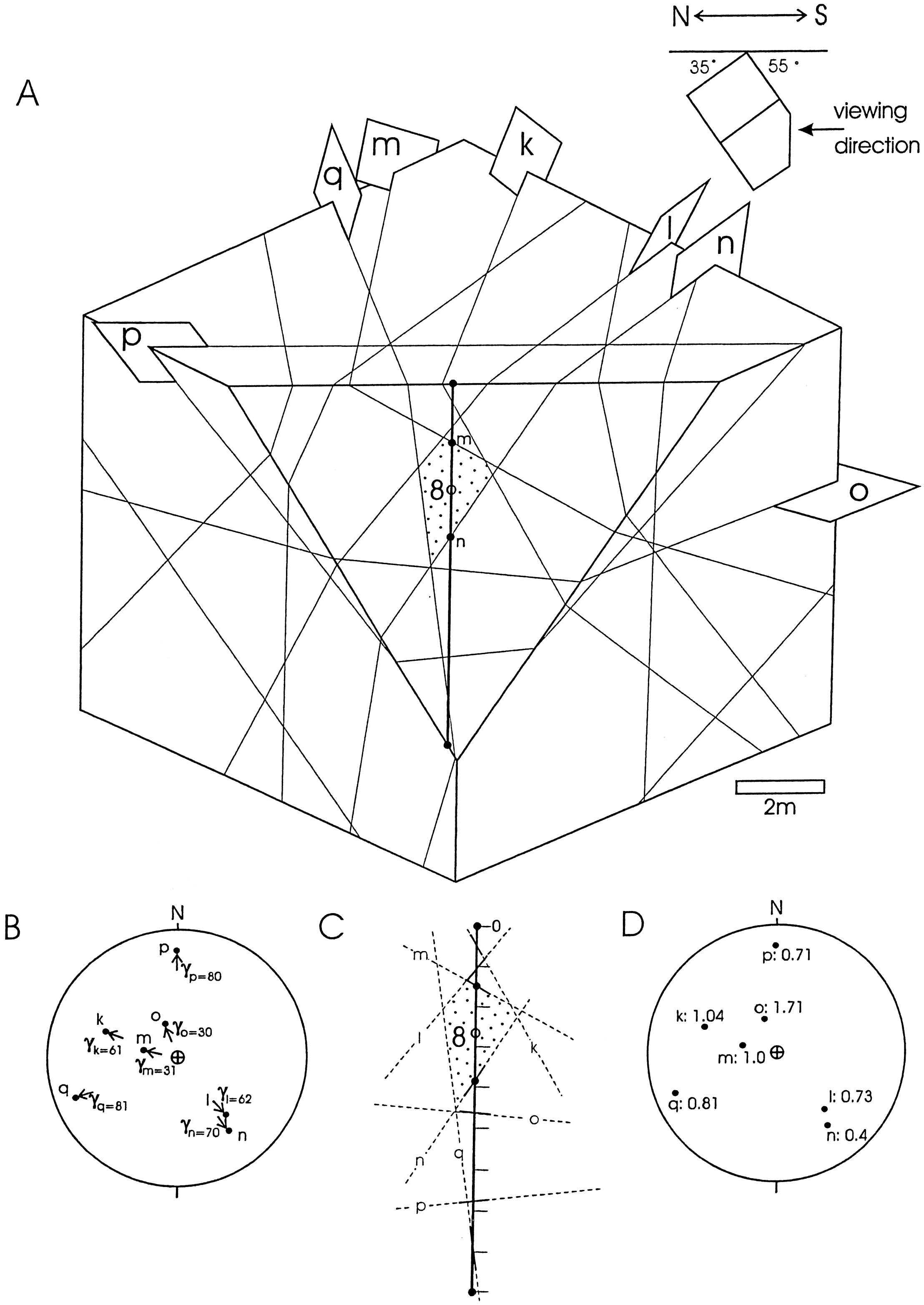

Fig. 8. (A) A schematic diagram of arbitrary discontinuity sets cut by a vertical plane (triangular face in centre) to show intersections with the discontinuities. An arbitrary vertical sample line (bold line with terminal bulbs) enters block 8 through face m and leaves through face n. (B) A stereograph (equal angle projection is used throughout) of discontinuities in (A) showing the angle between poles to faces and the vertical sample line (γ). (C) An extract from (A) showing the construction of block 8 (stippled) from intersections of neighbouring discontinuities (dashed lines) along the sample line. Intersections are labelled as for Figs. 6 and 7. (D) A stereograph showing the orientation of intersected discontinuities and their perpendicular distance (metres, see Table 1) from the 'eye' (mid point between m and n) of block 8. This diagram summarizes the shape and size of the block. The lack of poles in the northeast quadrant indicates the need to extend the sample line to 'close' the block.

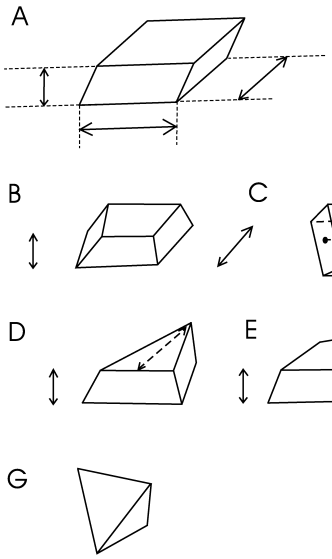

Fig. 9. (A) A parallelepiped block defined by three regular dimensions (arrows). (B) and (C) A block with two pairs of parallel faces has two regular dimensions (arrows) which can be augmented by the average separation of the remaining faces (dashed line with solid circles). (D)–(F) Blocks with one pair of parallel faces approximate triangular, quadrilateral or pentagonal prisms. (G) Blocks with no parallel faces can have a wide range of shapes including tetrahedra.

three orthogonal discontinuity sets), very blocky (multi-faceted angular blocks defined by four or more discontinuity sets), blocky/disturbed (folded and/or faulted with angular blocks formed by many intersecting discontinuity sets) and disintegrated. These descriptive classes form a trend of decreasing interlocking of the rock pieces.

The mechanical implications for these structural types and the degree of interlocking of blocks have many corollaries in structural geology. For example, brittle fault zones often show a similar range of fracture intensity. The localization of strain within faults confirms that as more fracture sets form and apertures between blocks are opened the resistance to deformation decreases.

One important contribution of structural geology is a comprehensive knowledge of three-dimensional patterns of discontinuities. Cross-cutting planar discontinuities such as joints have been well documented in the structural and engineering geology literature. In contrast, the engineering implications of anastomose patterns of discontinuities have not been fully developed. A variety of geological structures can display anastomosing patterns including the hinge zones of kinks in finely layered rocks (Stewart and Alvarez, 1991). Most commonly, anastomosing patterns are associated with faults and shear zones and have been reported in a range of settings including strike-slip duplexes (Woodcock and Fischer, 1986; Cruikshank et al., 1991; Laney and Gates, 1996), thrusts (Aerden, 1991; Watkinson, 1993), faults related to folding (Tanner, 1992), oblique convergence (Polinski and Eisbacher, 1992), extension (Power and Tullis, 1989; Varga, 1991), shearing in serpentinite (Gates, 1992), and analogue models of faulting (Tchalenko, 1968; Naylor et al., 1986; Smith and Durney, 1992).

Anastomosing fracture systems evolve with time (Cowie and Scholz, 1992) and the anastomosing morphology of faults is thought to be a result of en échelon fault segments being ‘out of phase’ (Craddock and Moshoian, 1995). Pre-existing fractures such as joints can play an important part in the development of the final structural pattern (Segall and Pollard, 1983; Martel, 1990). As fracture systems evolve the interconnecting networks also can control fluid migration (Marquer and Burkhard, 1992).

Previous work has focused on attempting to understand the mechanism of braided or anastomosing systems but less attention has been applied to making a clear statement of the geometry of these structures. The importance of geometrical characterization in the process of structural analysis is well illustrated by the role of geometric analysis of folds (e.g. Ramsay, 1967). In addition to developing a systematic non-genetic descriptive terminology, the reasons are two-fold. (1) For many geological purposes (spatial prediction) the geometric nature of a structure is needed. For example, in folding wavelength and amplitude of a fold system can be used in exploration for anticlinal traps or saddle reef veins. (2) Once systematic geometric parameters are identified kinematic and dynamic interpretations can focus on specific geometric features requiring mechanistic explanation.

Roughness exists on a range of scales and grades into what is often referred to as the waviness of a surface. The prime significance of waviness is that the effective angle of sliding is associated with the lowest angle parts of a wavy surface. Thus the average dip of a surface is typically adjusted by the waviness to give an effective dip angle. Likewise the basic friction angle of rock surfaces measured in a laboratory can be adjusted upward by an angle related to the roughness or waviness of the in situ surface.

The geological controls on roughness, such as plumose fracture marks, have received more attention than geological controls on surface waviness. In joint systems, curved stress trajectories can produce wavy systems of joint surfaces. In fault systems, waviness is a result of the anastomose patterns of branching and braided fault segmentation. The persistence, continuity and length of discontinuities form a group of parameters that are explicitly addressed in the RMR system but not in the other systems.

4. Determining size and shape of blocks

In data collection methods, such as field mapping and core logging, emphasis is commonly placed on identifying discontinuities that dissect the rock. Estimates of block shapes and sizes can be made from data on discontinuity sets and their spacing. However, with non-oriented core samples that approach is not possible. A complementary approach is to record the way local discontinuities define the geometry

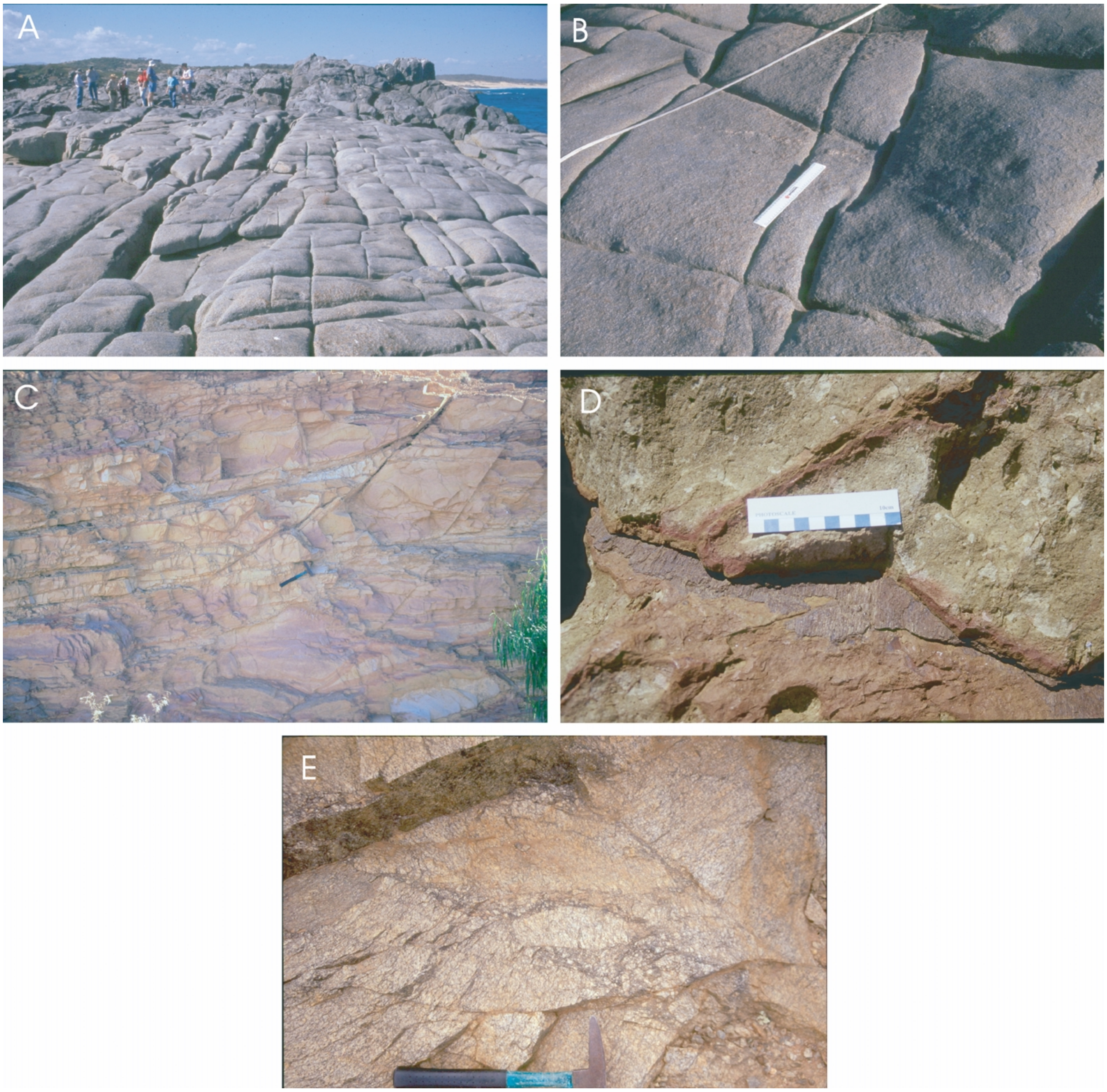

Fig. 10. (A) Dominant orthogonal joint patterns at Bingie Bingie Point South Coast New South Wales. (B) Detail of (A) shows more local variation (30 cm scale in centre). (C) Thrust fault system in a vertically bedded and cleaved metasiltstone, Cobar, western New South Wales. (D) Detail from (C) showing quartz–hematite slickenfibres on faults. (E) Oblique slip faults (and localized breccia) in foliated granite, Nymagee, western New South Wales.

of polygonal blocks that comprise the rock mass. Within a core sample intact lengths of core (core sticks; Franklin et al., 1971) are segments of individual blocks. Estimating the block size distributions from linear samples has similarities to stereological problems of textural analysis (e.g. Heilbronner and Bruhn, 1998); however, the data derived is three-dimensional.

A segment of core bounded by discontinuities (core stick) represents part of a block and the orientation of each terminal surface represents a face of the sampled block (Fig. 3A). Orientation data is commonly compiled for orientation analysis on a stereograph. A complimentary approach is to combine orientation and spacing data by plotting a graph of dihedral angle versus spacing of sequential pairs of discontinuities along a core. Assuming that discontinuities have persistence beyond individual blocks, other intersections in the neighbourhood of the core stick will also represent faces of the block (Fig. 3B). In this two-dimensional example, neighbouring discontinuities can be projected until a closed block is defined. By projecting a

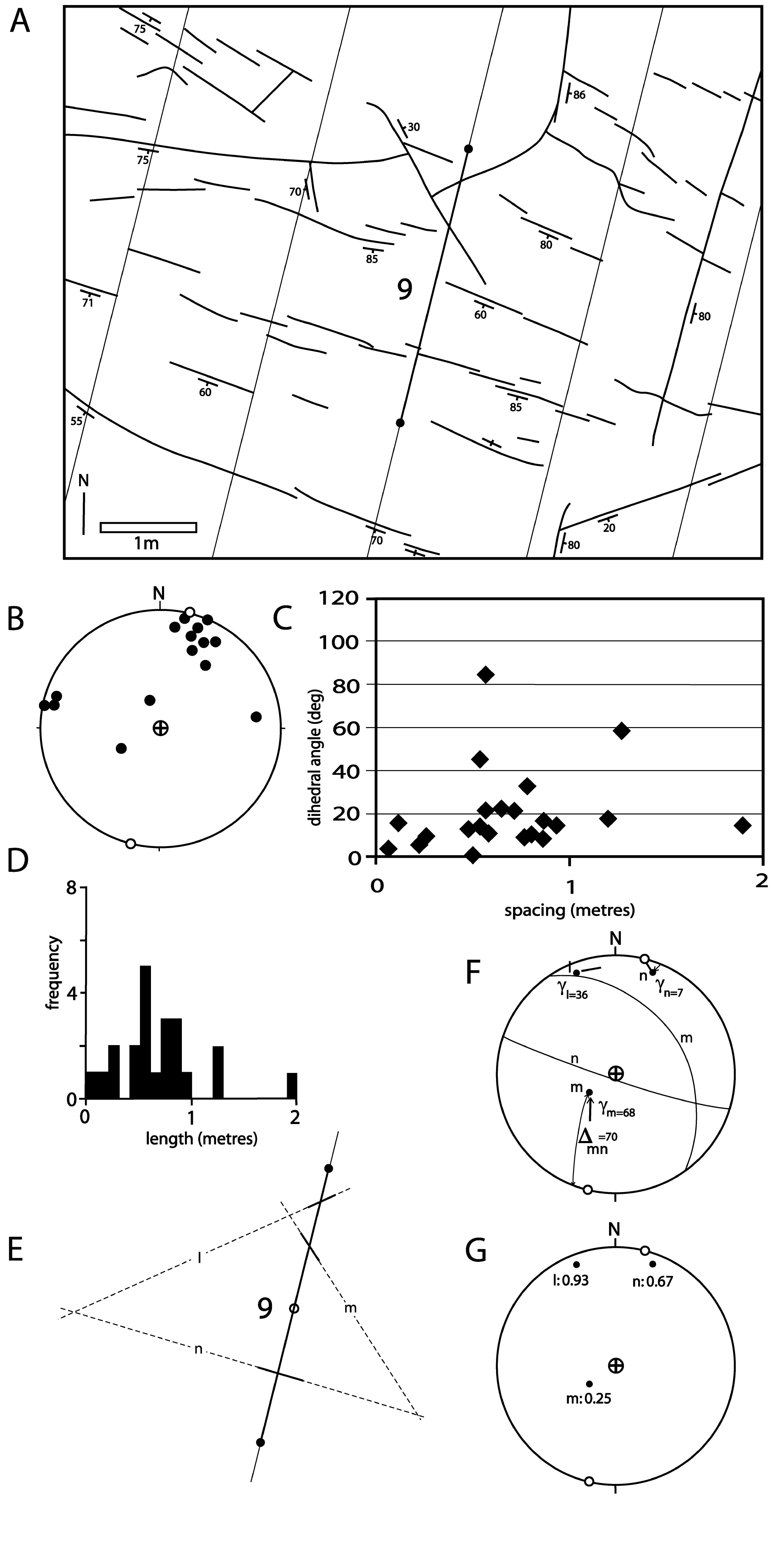
A
75
75
70
30
86
85
80
9
71
60
80
60
85
55
N
1m
70
20
80
B
N
C
120
100
80
60
40
20
0
dihedral angle (deg)
0
1
2
spacing (metres)
D
8
4
0
frequency
0
1
2
length (metres)
E
l
m
n
9
F
N
l
n
$\gamma_{l=36}$
$\gamma_{n=7}$
m
n
m
$\gamma_{m=68}$
$\Delta_{mn}=70$
G
N
l: 0.93
n: 0.67
m: 0.25

large number of neighbouring discontinuities bounding faces can be identified and a minimum size block can be defined.

An arbitrary reference point from which all enclosing surfaces can be measured is the mid-point of the core stick and will be referred to as the 'eye' of the block. The distance (D) along the core from the eye of the block to an intersection can be converted to an orthogonal distance (D') using the angle between the core axis and the pole to the plane (γ) (Fig. 3C):

$$D' = D\cos\gamma \quad (1)$$

These parameters are routinely collected in most structural core logging.

4.1. Two-dimensional model data

To illustrate data that can be obtained from recording the dihedral angle between sequential discontinuities and their corresponding spacing, simple two-dimensional models are presented. In each case a pattern of discontinuities is shown and arbitrary parallel sample lines represent a linear sampling (analogous to drill core) through the pattern. Scaled data are then represented graphically. For a regular orthogonal discontinuity system with near-constant discontinuity spacing (Fig. 4A and B) intervals less than the discontinuity spacing have dihedral angles at 90°, whereas the maximum spacings occurs for parallel structures. Individual blocks can be constructed from the set of neighbouring intersections (Fig. 4C). For a regular oblique discontinuity system with near-constant discontinuity spacing (Fig. 4D–F) a similar graph is obtained but with the intersected angle (acute in this case) shown. For irregularly spaced (Fig. 4G–I) and unequally represented (Fig. 4J–L) oblique discontinuity systems the graphs show variation in the spacing and number of parallel versus oblique structures. For a regular anastomose discontinuity system (Fig. 4M and N) a distinctive pattern comprising an arc with the maximum dihedral angle at an intermediate spacing is produced. Construction of the block from neighbouring intersections, assuming planar fractures, will only approximate the actual block shape (Fig. 4O).

4.2. Three-dimensional model data

In three-dimensions similar principles apply but it is necessary to use a stereograph to represent the orientations of bounding faces. From orientation alone it is not obvious whether an acute (Fig. 5A) or obtuse (Fig. 5B) corner has been intersected. For an acute intersection the sample line (Fig. 5C, circle) will lie in the obtuse field between the two planes (Fig. 5C, unstippled) whereas for an obtuse intersection the sample line will lie within the acute field between the two planes (Fig. 5D).

In natural rock masses discontinuities within sets commonly depart from parallelism and 'random' discontinuities are commonly present. Before giving examples of natural rock masses three model examples will be described. First, three orthogonal sets, second, four 'octahedral' sets and third, an arbitrary collection of discontinuities. The first two examples of regular systems of discontinuities are relatively trivial since reliable block shape and size distributions can be determined from orientation and spacing data. Blocks fully enclosed by discontinuities can be identified from stereographs. For random or arbitrary discontinuity distributions it is more difficult to identify which neighbouring discontinuities form the boundaries of each block. However, inferences can be made on the basis of stereographs and considerations of the range of possible block shapes.

Discontinuities can be projected in three-dimensions to determine the sizes and shapes of blocks along a linear sample. For regular discontinuity patterns the blocks have regular closed shapes that can be readily identified. For less predictable distributions, as expected in nature, closure of blocks is not as easily defined but is assisted by plotting a stereograph of neighbouring discontinuities. Blocks can lack closure if only a single orientation of discontinuities is intersected or if all discontinuities share a common axis. Blocks may appear to lack closure if the sample line fails to intersect bounding surfaces either because of inadequate sample length or a sampling orientation parallel to a discontinuity set. It is anticipated that a computerized version of this analysis will be needed to scan through the intersections to find those that define minimal volume blocks.

An arbitrary sample line through a system of orthogonal discontinuities intersects a number of blocks (Fig. 6A). The orientations of block faces relative to the sample line can be represented on a stereograph (Fig. 6B). Any chosen block (e.g. block 6; Fig. 6C) is enclosed by discontinuities in the neighbourhood of the sampled part of the block. These neighbouring intersections can be shown on a stereograph together with their perpendicular distance from the centre of the block intersection (Fig. 6D; Table 1). In this example, full enclosure is confirmed by the presence of pairs of planes

Fig. 11. (A) Detailed map of joints in tonalite, Bingi Bingi Point, South Coast New South Wales with arbitrary sample lines (fine lines). (B) A stereograph (equal angle used throughout) of joint orientations (solid circles) and sample line orientation (open circle). (C) Graph of dihedral angle versus spacing length for sequential intersections along the sample lines. (D) Histogram of intersection spacing (not corrected for orientation). (E) Construction of block 9 from neighbouring intersections. The low persistence of the joints limits the accuracy. (F) A stereograph showing the orientation of bounding faces of block 9. (G) A stereograph summarizing the orientation and perpendicular distance of faces (measured according to Fig. 3).

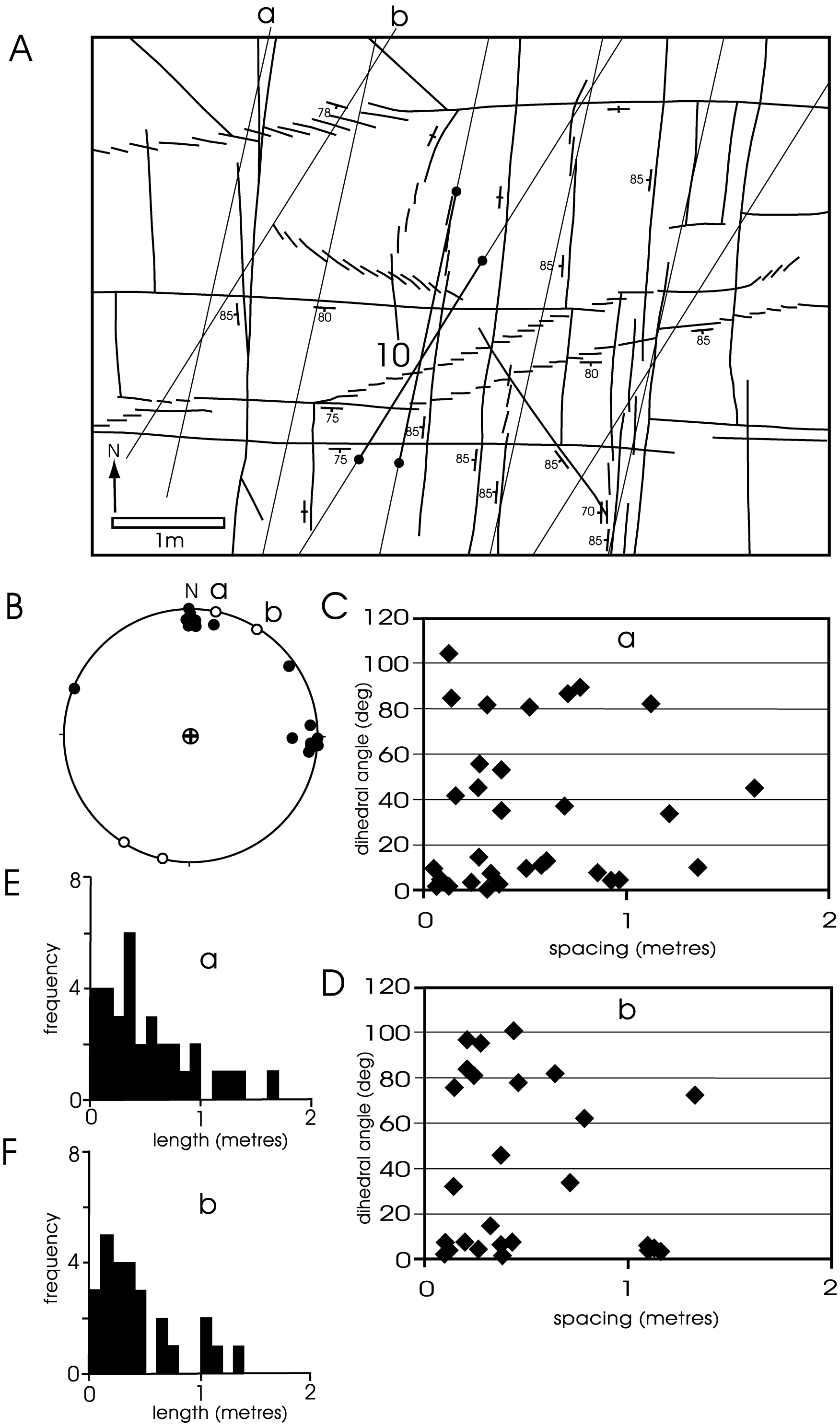

Fig. 12. (A) Detailed map of joints in granite, Tarandore Point, South Coast New South Wales with two sets of arbitrary sample lines (fine lines, a and b). (B) A stereograph (equal angle used throughout) of joint orientations (solid circles) and sample line orientation (open circle). (C) and (D) Graphs of dihedral angle versus spacing length for sequential intersections along sample lines a and b. (E) and (F) Histograms of intersection spacing (not corrected for orientation) for sample lines a and b. (G) and (H) Constructions of block 10 from neighbouring intersections for sample lines a and b, respectively. The low persistence of the joints limits the accuracy. (I) and (J) Stereographs showing the orientation of intersections in the neighbourhood of block 10 for each of the arbitrary sample lines. The bounding intersections (m and n) are also shown as great circles with the acute field stippled. (K) and (L) Stereographs showing the orientation (poles) and perpendicular distance in metres for the group of surfaces that partially enclose block 10 as determined by the two arbitrary sample lines.

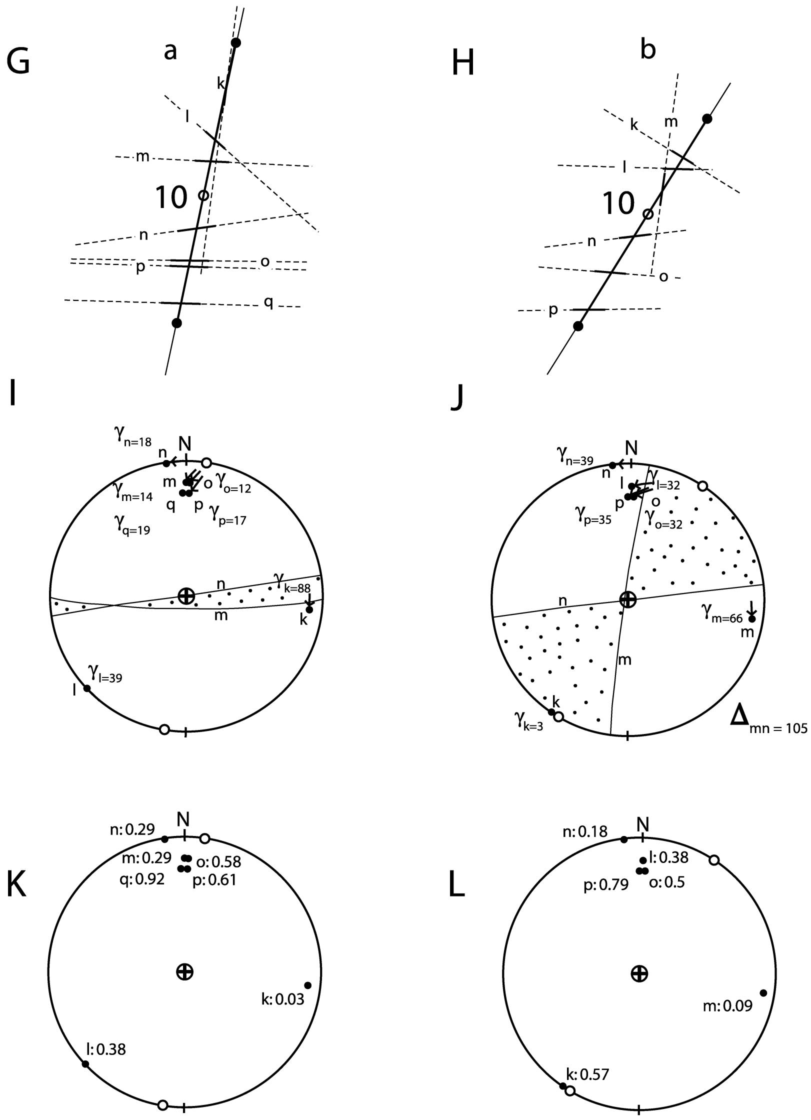

Fig. 12 (*continued*)

above and below the intersection in each orientation. A redundant plane (labelled ‘p’; Fig. 6D) can also be readily recognized.

Another regular system comprises discontinuities in four sets of orientations which intersect to form shapes including octahedra and tetrahedral (Fig. 7A). The orientations of block faces relative to the sample line can be represented on a stereograph (Fig. 7B). Any chosen block (e.g. block 7; Fig. 7C) is enclosed by discontinuities in the neighbourhood of the sampled part of the block. These neighbouring intersections can be shown on a stereograph together with their perpendicular distance from the centre of the block intersection (Fig. 7D; Table 1). In this example, the block is tetrahedral with full enclosure confirmed by the distribution of planes on the stereograph.

For an arbitrary collection of discontinuities (Fig. 8A) neighbouring intersections can be recorded on a stereograph (Fig. 8B). Any chosen block (e.g. block 8; Fig. 8C) is at least partially enclosed by the neighbouring intersections. A stereograph with poles and perpendicular distances to neighbouring planes provides a summary of the block size and shape (Fig. 8D; Table 1). The block has two sub-parallel faces with a perpendicular dimension of 1.13 m (planes l and n; Fig. 8D). The remaining faces are formed by five additional planes inclined between 30 and 90° to the sub-parallel faces.

Measurement of block dimensions, and therefore volumes, is dependent on shape. Any parallelepiped can be determined by the dimension of the parallel faces (Fig. 9A). Where two pairs of parallel faces exist these two dimensions can be augmented by an average separation of the non-parallel faces (Fig. 9B and C). Where one pair of parallel faces occurs this dimension can be augmented by combining the perpendicular distances to faces using different algorithms for triangular, quadrilateral and

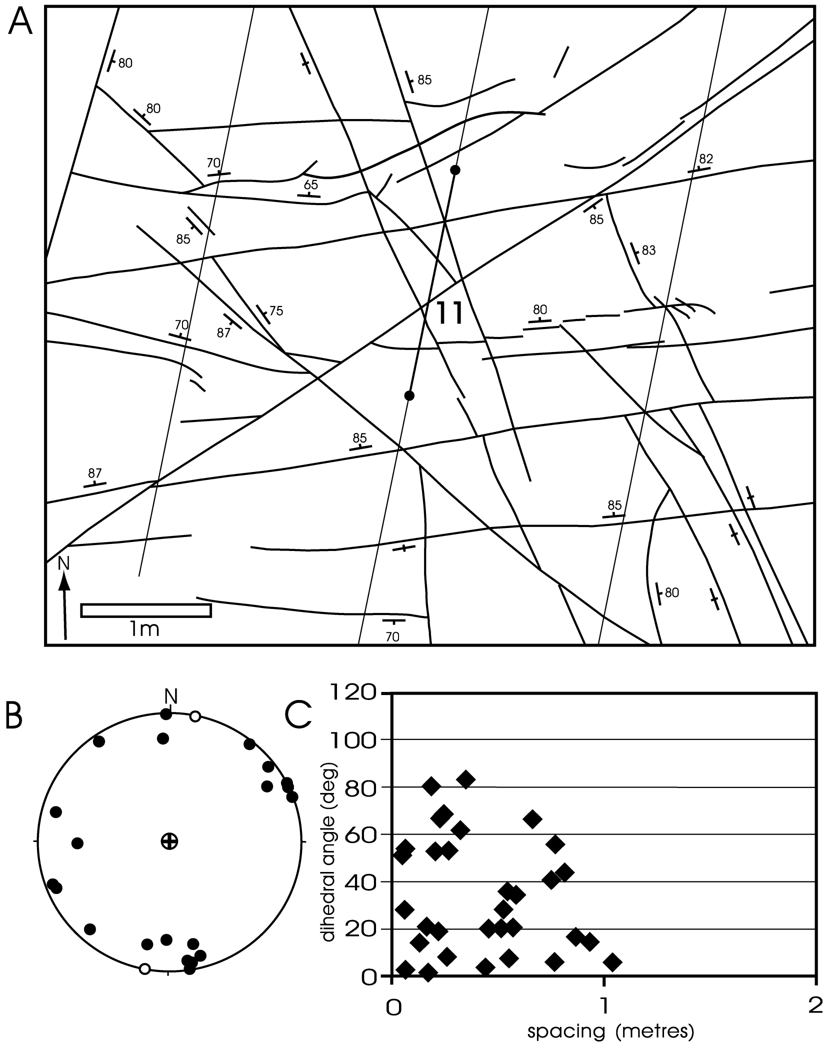

Fig. 13. (A) Detailed map of joints in diorite, Bingi Bingi Point, South Coast New South Wales with arbitrary sample lines (fine lines). (B) A stereograph (equal angle used throughout) of joint orientations (solid circles) and sample line orientation (open circle). (C) Graph of dihedral angle versus spacing length for sequential intersections along the sample lines. (D) Histogram of intersection spacing (not corrected for orientation). (E) Construction of block 11 from neighbouring intersections. The low persistence of the joints limits the accuracy. (F) A stereograph showing the orientation of bounding faces of block 11. (G) A stereograph summarizing the orientation and perpendicular distance of faces (measured according to Fig. 3).

pentagonal slabs (Fig. 9D–F). Shapes lacking parallel faces will require differing algorithms depending on their number of faces and angles between faces (e.g. tetrahedral; Fig. 9G).

4.3. Field examples

In order to further demonstrate the approach to estimating block size and shape from linear data a range of field examples are presented. Detailed maps of joints in granitic rocks of South Coast New South Wales, Australia (Fig. 10A and B) and faults in metamorphic and plutonic rocks of western New South Wales, Australia (Fig. 10C–E) were prepared and artificially sampled in a manner similar to the model data presented above.

The plutonic rocks exposed at Bingie Bingie Point and Tarandore Point are part of the Tuross Head Tonalite of the Moruya Batholith. The intimate association of felsic and mafic magmatic rocks has been interpreted as the result of synplutonic mingling of distinct magma compositions (Vernon et al., 1988; Keay et al., 1997). Detailed mapping of the orientations and pattern of joints at Tuross Heads and Bingi Bingi Point will be described. Areas approximately 6 m by 5 m were mapped at a scale of 1:50 (Figs. 11A, 12A and 13A). Arbitrary linear samples of dihedral angle and spacing of sequential joints were derived from the maps. The three-dimensional orientation of joints is recorded but the sample line is parallel to a major joint orientation. Therefore, it is the shapes and sizes of blocks in the mapped surface that is considered here, rather than a full three-dimensional analysis.

Joints in tonalite at Bingi Bingi Point (Fig. 11A) comprise one dominant joint set parallel to the magmatic foliation of the rock. The system comprising 1 set with random joints would be given a J_n value of 3. The

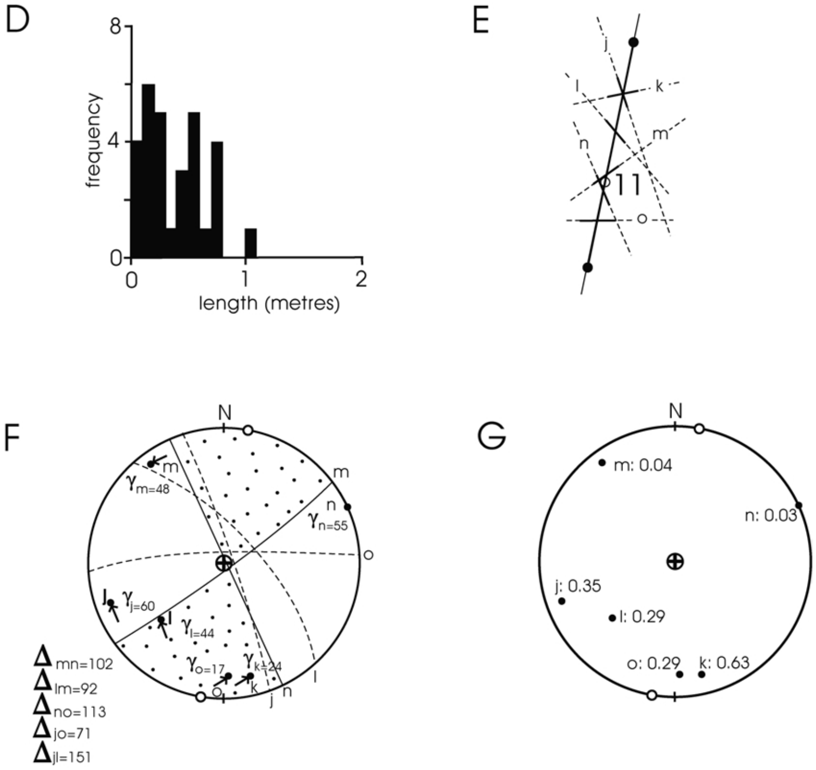

Fig. 13 (*continued*)

stereograph (Fig. 11B) shows the clustering of joints in three dimensions. The graph of dihedral angle versus spacing (Fig. 11C) shows a concentration of intersections at low dihedral angles. From the graph and histogram (Fig. 11D) it can be interpreted that the rock mass comprises slab-shaped blocks ranging in thickness up to 2 m but most commonly about 0.8 m thick. A construction of block 9 from intersections would incorrectly assume continuity of surface l (Fig. 11E). Stereographs of the orientation and perpendicular distance to inferred bounding surfaces (Fig. 11F and G) show a lack of block closure caused by the dominance of a single set of discontinuities.

Joints in tonalite at Tarandore Point (Fig. 12A) comprise two dominant orthogonal joint sets with random joints and en échelon joint arrays (a third orthogonal set parallel to the mapped face is not shown). The system (as sampled) comprising 2 sets with random joints would be given a J_n value of 6. The stereograph (Fig. 12B) shows the clustering of joints in three dimensions. This discontinuity population was sampled along two arbitrarily oriented lines for comparison. In both, dihedral angle versus spacing graphs (Fig. 12C and D), concentrations of intersections at a low dihedral angle and at 90° occur along with intermediate angles. From the graphs and histograms (Fig. 12E and F) it can be interpreted that the rock mass comprises mainly rectangular prismatic blocks ranging in size up to 1.5 m but most commonly less than 1 m in size. The uneven distribution between low and high dihedral angles implies a rectangular rather than square profile shape of the blocks. An arbitrary block (block 10; Fig. 12G and H) can be partly constructed from intersections in the short linear sample.

Stereographs of the orientations (Fig. 12I and J) and distances (Fig. 12K and L) summarize the size and shape of the block. The block has one pair of sub-parallel faces separated by approximately 0.57 m. There is an apparent lack of block closure by sub-horizontal surfaces (resulting from the sample line being parallel to a discontinuity set). There is also an apparent lack of block closure to the west because the sample line was insufficiently long to intersect the north–south striking discontinuity to the west. A number of redundant surfaces would be intersected prior to the bounding surface being located.

Joints in diorite at Bingi Bingi Point (Fig. 13A) comprise one dominant joint set with another possible set and numerous other orientations (a third orthogonal set parallel to the mapped face is not shown). The system comprising 1 (or 2) set with random joints would be given a J_n value of 3 (or 6). The stereograph (Fig. 13B) shows the distribution of joints in three dimensions. The graph of dihedral angle versus spacing (Fig. 13C) shows a wide distribution of angles (not exceeding 82°) and spacing. From the graph and histogram (Fig. 13D) it can be interpreted that the rock mass comprises triangular and trapezoidal prisms and/or tetrahedra ranging in size up to 1 m. An arbitrary block (block 11 in Fig. 13E) can be constructed from neighbouring intersections. Stereographs of the orientations (Fig. 13F)

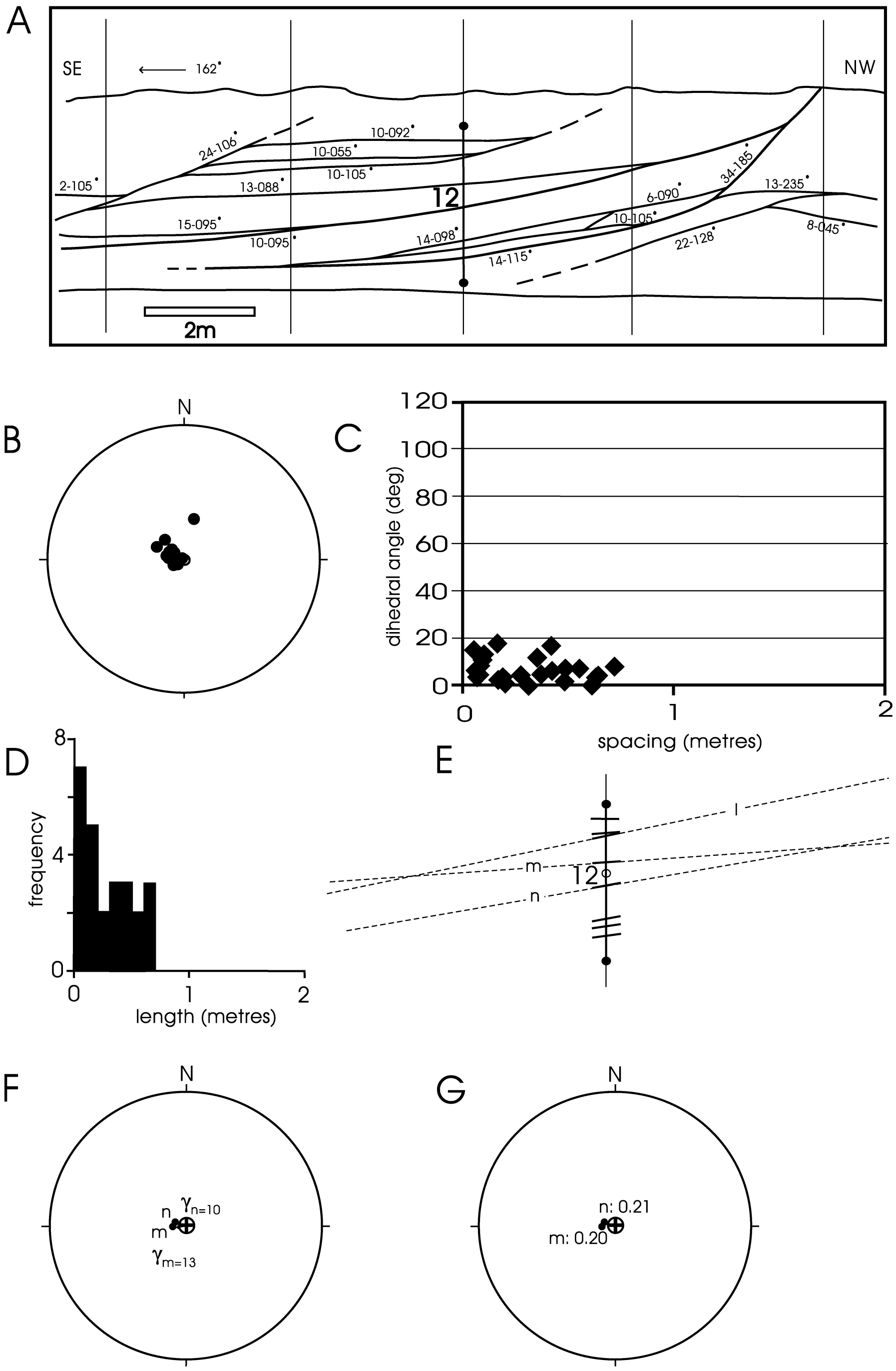

Fig. 14. (A) Detailed map of thrust faults in metasiltstone, Cobar, western New South Wales. (B) A stereograph (equal angle used throughout) of joint orientations (solid circles) and sample line orientation (open circle). (C) Graph of dihedral angle versus spacing length for sequential intersections along the sample lines. (D) Histogram of intersection spacing (not corrected for orientation). (E) Construction of block 12 from neighbouring intersections. (F) A stereograph showing the orientation of bounding faces of block 12. (G) A stereograph summarizing the orientation and perpendicular distance of faces (measured according to Fig. 3).

and perpendicular distances (Fig. 13G) show that block 11 is bounded by a pair of sub-parallel faces (j and n in Fig. 13G) separated by 0.38 m. The block appears to lack closure in the vertical direction because the sample lines are parallel to a set of sub-horizontal discontinuities.

Thrust faults in meta-siltstones Cobar western New South Wales were mapped in profile along a railway cutting (Fig. 14A;/ Smith and Marshall, 1992). This example comprises anastomosing discontinuity surfaces. Bedding and sub-parallel cleavage are oriented approximately parallel to the exposed face and not intersected by the vertical sample lines. The stereograph (Fig. 14B) shows the strong clustering of joints in three dimensions. The graph of dihedral angle versus spacing (Fig. 14C) shows a strong

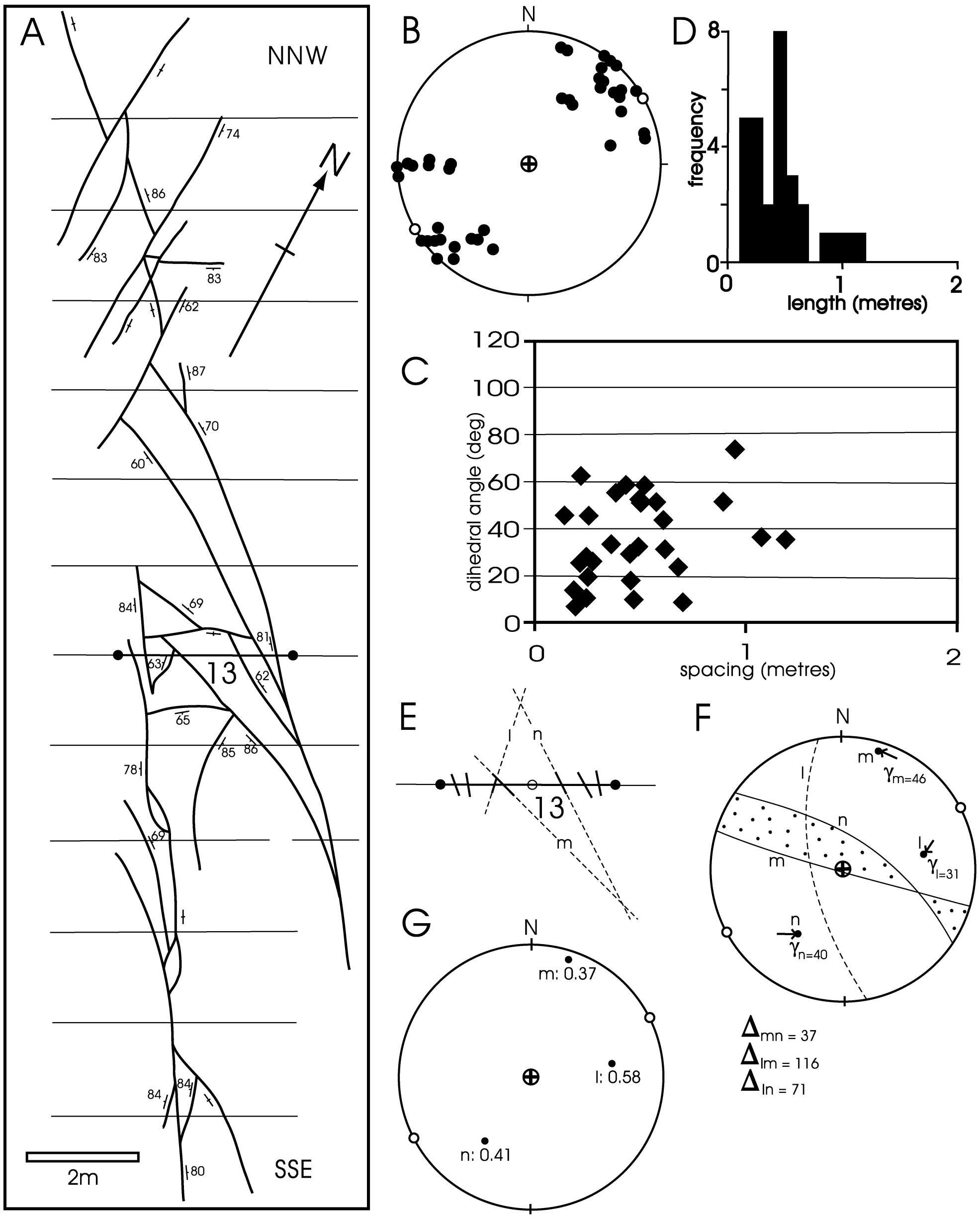

Fig. 15. (A) Detailed map of oblique faults in foliated granite, Nymagee western New South Wales. (B) A stereograph (equal angle used throughout) of joint orientations (solid circles) and sample line orientation (open circle). (C) Graph of dihedral angle versus spacing length for sequential intersections along the sample lines. (D) Histogram of intersection spacing (not corrected for orientation). (E) Construction of block 13 from neighbouring intersections. (F) A stereograph showing the orientation of bounding faces of block 13. (G) A stereograph summarizing the orientation and perpendicular distance of faces (measured according to Fig. 3).

concentration of intersections at a low dihedral angle. From the graph and histogram (Fig. 14D) it can be interpreted that the rock mass comprises slab-shaped blocks ranging in thickness up to 0.75 m. An arbitrary block (block 12 in Fig. 14E) can be constructed from neighbouring intersections. Stereographs of the orientations (Fig. 14F) and perpendicular distances (Fig. 14G) show that block 12 is bounded by a pair of sub-parallel faces (m and n in Fig. 14G) separated by 0.41 m. The lateral extension of the block can be estimated by the distances at which the sub-parallel planes would intersect.

Oblique slip chlorite–epidote faults zones in granite of the Nymagee Igneous Complex in western New South Wales were mapped along a road cutting (Fig. 15A). This example comprises a combination of cross-cutting and anastomose discontinuity surfaces. The stereograph (Fig. 15B) shows the distribution of joints in three dimensions. The graph of dihedral angle versus spacing (Fig. 15C) shows a wide distribution of angles (not exceeding 77°) and spacing. From the graph and histogram (Fig. 15D) it can be interpreted that the rock mass comprises triangular and trapezoidal prisms and/or tetrahedra ranging in size up to

1.2 m but mainly less than 0.75 m. An arbitrary block (block 13 in Fig. 15E) can be constructed from neighbouring intersections. Stereographs of the orientations (Fig. 15F) and perpendicular distances (Fig. 15G) show that block 13 is bounded by a tetrahedral wedge closing upward (l–n in Fig. 15G).

5. Conclusions

Geotechnical rock mass assessment methods aim to reduce data by combining parameters to derive quasi-physical parameters or arbitrary scores. An important parameter is the size and shape of the blocks of rock which comprise the rock mass. A new approach to measurement of block sizes and shapes is obtained by collating dihedral angle versus spacing of sequential discontinuities in linear samples. In drill core (whether oriented or not) the method is applied by measuring the length and dihedral angles between the terminal faces of intact pieces of core. The data provides data on the shape and size of blocks of rock between discontinuities. The method can be extended to construct individual blocks from the orientation of neighbouring intersections. Blocks can be represented on a stereograph allowing their shapes and sizes to be determined. In particular, blocky to very blocky structures within the GSI classification scheme can be recognized and accurately determined. The approach is more closely related to physical features than the commonly used RQD versus J_n approach. Identifying the size and shape of specific blocks rather than relying on statistical methods is beneficial to critical aspects of design such as analysing keyblocks that would be exposed during excavations. The detailed characterization of block size and shape is also a step toward interpreting the kinematics of rock mass deformation and the analysis of rock masses as ultra-close packed dilatant granular systems.

Acknowledgements

James Maslen (RMIT) provided helpful discussion on many aspects of rock mass assessment and classification. This paper benefited from review comments by Norman Fry and an anonymous reviewer with editorial oversight from Julian Vearncombe.

References

Aerden, D.G.A.M., 1991. Foliation-boudinage control on the formation of the Rosebery Pb–Zn orebody, Tasmania. Journal of Structural Geology 13, 759–775.

Afrouz, A.A., 1992. Practical Handbook of Rock Mass Classification Systems and Modes of Ground Failure. CRC Press Inc, Boca Raton.

Barton, N., 1999. General report concerning some 20th century lessons and 21st century challenges in applied rock mechanics, safety and control of the environment. In: ISRM Congress, Paris, pp. 1–22.

Barton, N., Lien, R., Lunde, J., 1974. Engineering classification of rock masses for the design of tunnel support. Rock Mechanics 6, 183–236.

Bieniawski, Z.T., 1989. Engineering Rock Mass Classifications. Wiley, New York.

Cameron-Clarke, I.S., Budavari, S., 1981. Correlation of rock mass classification parameters obtained from borecore and in-situ observations. Engineering Geology 17, 19–53.

Carranza-Torres, C., Fairhurst, C., 1999. The elasto-plastic response of underground excavations in rock masses that satisfy the Hoek–Brown failure criterion. International Journal of Rock Mechanics and Mining Sciences 36, 777–809.

Cowie, P.A., Scholz, C.H., 1992. Physical explanation for the displacement–length relationship of faults using a post-yield fracture mechanics model. Journal of Structural Geology 14, 1133–1148.

Craddock, J.P., Moshoian, A., 1995. Continuous Proterozoic strike-slip fault–en echelon fracture arrays in Archean rocks: implications for fault propagation mechanics and dike injection. Basement Tectonics 10, 379–407.

Cruikshank, K.M., Zhao, G., Johnson, A.M., 1991. Duplex structures connecting fault segments in Entrada sandstone. Journal of Structural Geology 13, 1185–1196.

Cunha, A.P., 1993. Research on scale effects in the determination of rock mass mechanical properties—the Portuguese experience. In: Cunha, A.P., (Ed.), Scale Effects in Rock Masses 93. Proceedings of the Second International Workshop on Scale Effects in Rock Masses, A.A. Balkema, Lisbon, pp. 133–141.

Engelder, T., Haith, B.F., Younes, A., 2001. Horizontal slip along Alleghanian joints of the Appalachian plateau. Tectonophysics 336, 31–41.

Fookes, P.G., 1997. Geology for engineers: the geological model, prediction and performance. Quarterly Journal of Engineering Geology 30, 293–424.

Franklin, J.A., Broch, E., Walton, G., 1971. Logging the mechanical character of rock. Transcriptions of the Institute of Mining and Metallurgy, London Section A81, A1–A9.

Fry, N., 2001. Stress space: striated faults, deformation twins and their constraints on paleostress. Journal of Structural Geology 23, 1–9.

Gapais, D., Cobbold, P.R., Bourgeois, O., Rouby, D., Urreiztieta, M., 2000. Tectonic significance of fault-slip data. Journal of Structural Geology 22, 881–888.

Gates, A.E., 1992. Domainal failure of serpentinite in shear zones, State–Line mafic complex, Pennsylvania, USA. Journal of Structural Geology 14, 19–28.

Gentier, S., Riss, J., Archambault, G., Flamand, R., Hopkins, D., 2000. Influence of fracture geometry on shear behavior. International Journal of Rock Mechanics and Mining Sciences 37, 161–174.

Guvanasen, V., Chan, T., 2000. A three-dimensional numerical model for thermohydromechanical deformation with hysterisis in a fractured rock mass. International Journal of Rock Mechanics and Mining Sciences 37, 89–106.

He, J., 1993. A case review of the deformation modulus of rock mass: scale effect. In: Cunha, A.P., (Ed.), Scale Effects in Rock Masses 93. Proceedings of the Second International Workshop on Scale Effects in Rock Masses, A.A. Balkema, Lisbon, pp. 87–91.

Heilbronner, R., Bruhn, D., 1998. The influence of three-dimensional grain size distributions on the rheology of polyphase rocks. Journal of Structural Geology 20, 695–705.

Hoek, E., Brown, E.T., 1997. Practical estimates of rock mass strength. International Journal of Rock Mechanics and Mining Sciences 34, 1165–1186.

Hopkins, D.L., 2000. The implications of joint deformation in analyzing the properties and behavior of fractured rock masses, underground excavations, and faults. International Journal of Rock Mechanics and Mining Sciences 37, 175–202.

Jing, L., 2000. Block system construction for three-dimensional discrete element models of fractured rocks. International Journal of Rock Mechanics and Mining Sciences 37, 645–659.

Jouniaux, L., Masuda, K., Lei, X.L., Nishizawa, O., Kusunose, K., Liu, L.Q., Ma, W.T., 2001. Comparison of the microfracture localization in granite between fracturation and slip of a preexisting macroscopic healed joint by acoustic emission measurements. Journal of Geophysical Research 106, 8687–8698.

Keay, S., Collins, W.J., McCulloch, M.T., 1997. A three-component Sr–Nd isotopic mixing model for granitoid gneisses, Lachlan fold belt, eastern Australia. Geology 25, 307–310.

Kulatilake, P.H.S.W., Malama, B., Wang, J., 2001. Physical and particle flow modeling of jointed block behavior under uniaxial loading. International Journal of Rock Mechanics and Mining Sciences 38, 641–657.

Kuszmaul, J.S., 1999. Estimating keyblock sizes in underground excavations: accounting for joint set spacing. International Journal of Rock Mechanics and Mining Sciences 36, 217–232.

La Pointe, P.R., Hudson, J.A., 1985. Characterization and interpretation of rock mass joint patterns. In: Special Publication 199. Geological Society of America.

Laney, S.E., Gates, A.E., 1996. Three-dimensional shuffling of horses in a strike-slip duplex: an example from the Lambertville sill, New Jersey. Tectonophysics 258, 53–70.

Lu, J., 2002. Systematic identification of polyhedral rock blocks with arbitrary joints and faults. Computers and Geotechnics 29, 49–72.

Maerten, L., Pollard, D.D., Maerten, F., 2001. Digital mapping of three-dimensional structures of the Chimney Rock fault system, central Utah. Journal of Structural Geology 23, 585–592.

Marquer, D., Burkhard, M., 1992. Fluid circulation, progressive deformation and mass-transfer processes in the upper crust: the example of basement-cover relationships in the External Crystalline Massifs, Switzerland. Journal of Structural Geology 14, 1047–1057.

Martel, S.J., 1990. Formation of compound strike-slip fault zones, Mount Abbot quadrangle, California. Journal of Structural Geology 12, 869–882.

Mauldon, M., 1995. Keyblock probabilities and size distributions: a first model for impersistent 2-D fractures. International Journal of Rock Mechanics and Mining Sciences and Geomechanics Abstracts 32, 575–583.

Mauldon, M., Dunne, W.M., Rohrbaugh, M.B., 2001. Circular scanlines and circular windows: new tools for characterizing the geometry of fracture traces. Journal of Structural Geology 23, 247–258.

Moon, H.-K., Kim, C.-Y., 1993. Scale effects in the elastic moduli and strength of jointed rock masses. In: Cunha, A.P., (Ed.), Scale Effects in Rock Masses 93. Proceedings of the Second International Workshop on Scale Effects in Rock Masses, A.A. Balkema, Lisbon, pp. 39–48.

Naylor, M.A., Mandi, G., Sijpesteijn, C.H.K., 1986. Fault geometries in basement-induced wrench faulting under different initial stress states. Journal of Structural Geology 8, 737–752.

Pariseau, W.G., 1999. An equivalent plasticity theory for jointed rock masses. International Journal of Rock Mechanics and Mining Sciences 368, 907–918.

Paterson, M.S., 1978. Experimental Rock Deformation—The Brittle Field. Springer-Verlag, Berlin.

Peacock, D.C.P., 2001. The temporal relationship between joints and faults. Journal of Structural Geology 23, 329–341.

Polinski, R.K., Eisbacher, G.H., 1992. Deformation partitioning during polyphase oblique convergence in the Karawanken Mountains, southeastern Alps. Journal of Structural Geology 14, 1203–1213.

Power, W.L., Tullis, T.E., 1989. The relationship between slickenside surfaces in fine-grained quartz and the seismic cycle. Journal of Structural Geology 11, 879–893.

Priest, S.D., 1993. Discontinuity Analysis for Rock Engineering. Chapman and Hall, London.

Ramsay, J.G., 1967. Folding and Fracturing of Rocks. McGraw-Hill, New York, 568pp.

Ranalli, G., 2000. Rheology of the crust and its role in tectonic reactivation. Journal of Geodynamics 30, 3–15.

Renard, F., Gratier, J.-P., Jamtveit, B., 2000. Kinetics of crack-sealing, intergranular pressure solution and compaction around active faults. Journal of Structural Geology 22, 1395–1407.

Schultz, R.A., 2001. Growth of geologic features into large strain populations: review of nomenclature, subcritical crack growth and some implications for rock engineering. International Journal of Rock Mechanics and Mining Sciences 37, 403–411.

Segall, P., Pollard, D.D., 1983. Nucleation and growth of strike slip faults in granite. Journal of Geophysical Research 88, 555–568.

Shen, B., Barton, N., 1997. The disturbed zone around tunnels in jointed rock masses. International Journal of Rock Mechanics and Mining Sciences 34, 117–125.

Sitharam, T.G., Sridevi, J., Shimizu, N., 2001. Practical equivalent continuum characterization of jointed rock mass. International Journal of Rock Mechanics and Mining Sciences 38, 437–448.

Smith, J.V., Durney, D.W., 1992. Experimental formation of brittle structural assemblages in oblique divergence. Tectonophysics 216, 235–253.

Smith, J.V., Marshall, B., 1992. Patterns of folding and fold interference in oblique contraction of layered rocks of the inverted Cobar Basin, Australia. Tectonophysics 215, 319–334.

Starzec, P., Andersson, J., 2002. Application of two-level factorial design to sensitivity analysis of keyblock statistics from fracture geometry. International Journal of Rock Mechanics and Mining Sciences 39, 243–255.

Stewart, K.G., Alvarez, W., 1991. Mobile-hinge kinking in layered rocks and models. Journal of Structural Geology 13, 243–259.

Streit, J.E., Cox, S.F., 2000. Asperity interactions during creep of simulated faults at hydrothermal conditions. Geology 28, 231–234.

Streit, J.E., Cox, S.F., 2002. Evolution of fracture networks in shear zones: insights from see-through experiments on biphenyl aggregates. Journal of Structural Geology 24, 107–122.

Tanner, P.W.G., 1992. Morphology and geometry of duplexes formed during flexural-slip folding. Journal of Structural Geology 14, 1173–1192.

Tchalenko, J.S., 1968. The evolution of kink-bands and the development of compression textures in sheared clays. Tectonophysics 6, 159–174.

Tsutsumi, H., Yeats, R.S., Huftile, G.J., 2001. Late Cenozoic tectonics of the northern Los Angelos fault system, California. Bulletin of the Geological Society of America 113, 454–468.

Varga, R.J., 1991. Modes of extension at oceanic spreading centers: evidence from the Solea graben, Troodos ophiolite, Cyprus. Journal of Structural Geology 13, 517–537.

Vermilye, J.M., Scholz, C.H., 1998. The process zone: a microstructural view of fault growth. Journal of Geophysical Research 103, 12223–12237.

Vernon, R.H., Etheridge, M.A., Wall, V.J., 1988. Shape and microstructure of microgranitoid enclaves: indicators of magma mingling and flow. Lithos 22, 1–11.

Watkinson, A.J., 1993. A footwall system of faults associated with a foreland thrust in Montana. Journal of Structural Geology 15, 335–342.

Wilkins, S.J., Gross, M.R., Wacker, M., Eyal, Y., Engelder, T., 2001. Faulted joints: kinematics, displacement–length scaling relations and criteria for their identification. Journal of Structural Geology 23, 315–327.

Woodcock, N.H., Fischer, M., 1986. Strike-slip duplexes. Journal of Structural Geology 8, 725–735.

Wu, F., Wang, S., 2001. A stress–strain relation for jointed rock masses. International Journal of Rock Mechanics and Mining Sciences 38, 591–598.

Zhang, L., Einstein, H.H., 2000. Estimating the intensity of rock discontinuities. International Journal of Rock Mechanics and Mining Sciences 37, 819–837.